International Journal of Robust and Nonlinear Control

WILEY

RESEARCH ARTICLE

Decentralized Finite-Time Adaptive Neural Output-Feedback Quantized Control for Switched Nonlinear Large-Scale Delayed Systems

Zhenhua Li[1,2] | Hongtian Chen[1] | Wentao Wu[1,2] | Zehua Jia[1,3] | Weidong Zhang[1,3]

[1]Department of Automation, Shanghai Jiao Tong University, Shanghai, China | [2]Hainan Research Institute, Shanghai Jiao Tong University, Sanya, China | [3]School of Information and Communication Engineering, Hainan University, Haikou, China

Correspondence: Weidong Zhang (wdzhang@sjtu.edu.cn)

Received: 18 October 2023 | **Revised:** 23 August 2024 | **Accepted:** 20 November 2024

Funding: This paper was supported in part by the National Science and Technology Major Project under Grant 2022ZD0119900, in part by the National Natural Science Foundation of China under Grant U2141234, Grant U24A20260, and Grant 62303308, in part by the Hainan Province Science and Technology Special Fund under Grant ZDYF2024GXJS003, in part by Shanghai Pujiang Program under Grant 23PJ1404700, in part by Joint Research Fund of Shanghai Academy of Spaceflight Technology under Grant USCAST2023-22, and in part by the Hainan Special PhD Scientific Research Foundation of Sanya Yazhou Bay Science and Technology City under Grant HSPHDSRF-2022-01-005.

Keywords: decentralized neural output-feedback quantized control | finite-time stability | multiple Lyapunov–Krasovskii functions | persistent dwell time | switched nonlinear large-scale delayed systems

ABSTRACT

This paper considers the problem of decentralized finite-time adaptive neural output-feedback quantized control for a class of switched nonlinear large-scale delayed systems. A switched high-gain quantized state observer is therefore constructed for each subsystem to estimate unavailable system states. Different from the traditional Lyapunov–Krasovskii functional method, multiple Lyapunov–Krasovskii functions are introduced to develop the decentralized adaptive output-feedback control strategy with neural network approximation for the switched nonlinear large-scale delayed systems. Under a category of switching signals with persistent dwell time, all signals in the closed-loop switched system are semi-globally uniformly ultimate bounded. Meanwhile, the tracking errors can remain in a small domain of origin in finite time. Case studies are finally used to illustrate the flexibility and effectiveness of the proposed control approach, including the switched two continuous stirred tank reactor delayed systems.

1 | Introduction

Neural networks have drawn extensive attention over the last decades due to their capability in universal approximation. In particular, adaptive neural network control has become one of the most popular tools for stability and stabilization of nonlinear systems [1–5]. Through online learning to modify the weights, the robustness and the convergence of the nonlinear systems can be improved by updating adaptive parameters. The neural networks-based backstepping technique is an effective adaptive control design strategy for nonlinear systems [6]. However, the explosion of dimensionality is often produced by repeating the differentiation of the virtual controller inputs in the backstepping technique. To address this issue, Reference [7] presented a dynamic surface control technique. In Reference [8], the modified dynamic surface control has been presented for the half-car active suspension systems by the adaptive neural controller. In Reference [6], the adaptive neural optimal control has been presented for nonlinear multi-agent systems via the dynamic surface control technique. In fact, due to the limitation

© 2024 John Wiley & Sons Ltd.

of the sensor, the system states are not always available during the operation. Besides, the aforementioned studies mostly focus on non-switched nonlinear systems. Therefore, it is expected to develop adaptive neural network control strategies for switched nonlinear systems under the output-feedback framework.

Especially, switched systems have attracted much more attention in the last decades [9–15]. They contain several subsystems and a switching signal, which can stand for lots of practical systems, such as single-link robots, chemical reactor systems, and circuit network systems in References [16–19]. In addition, one key issue in the stability problem of switched systems is to design a suitable switching signal. At present, some significant design approaches for switched systems have been reported, such as the common Lyapunov function, dwell time, multiple Lyapunov function, and average dwell time [12, 18, 19]. Meanwhile, it is worth noting in Reference [20] that the persistent dwell time switching is more general since both dwell time and average dwell time are regarded as special switching cases. The persistent dwell time switching strategy has been reported for the stabilization of switched linear systems [21], switched nonlinear systems [22], and saturated switched delay systems [23]. In the practical application of switched systems, it is inevitable to suffer from the change of controllable variable lags (also named time delays), owing to long transmission lines and self-physical characteristics.

Otherwise, the time delays can worsen the system performance index and even result in the instability of control systems. In general, the Lyapunov–Krasovskii function method and the Lyapunov-Razumikhin method are the two significant methods to address the stability problem of delayed systems in References [15, 24–28]. Currently, most of the existing control strategies under the persistent dwell time switching for the switched nonlinear delayed systems cannot be applied to the digital channel with limited communication bandwidth since these methods are set up in the framework of continuous-time feedback control. Besides, to reduce the impact of some possible constraints on information-processing devices, the quantized control strategy has been proposed due to its capacity with a finite number of data bits [29–32]. Naturally, this study focuses on developing the various adaptive neural output-feedback quantized control strategies for switched nonlinear large-scale delayed systems with data rate constraints.

Remarkably, finite-time stability has attracted considerable attention and achieved many significant results due to its finite-time convergence for practical control systems, such as the electro-hydraulic servo system [33], the complex dynamical networks [34], the pendulum system [35], and the vehicle system [36]. In the existing results, the control purpose of the finite-time stabilization for the nonlinear systems is often to design the control strategies such that system states can stay in the small domain of the origin in the finite time. In Reference [37], based on an improved disturbance observer, the fixed-time consensus tracking strategy was proposed for multi-agent systems. The command filtering-based finite-time tracking control was developed for switched nonlinear systems with a hysteresis input under arbitrary switching in Reference [38]. Moreover, the nonlinear system under finite-time stability has stronger robustness than that with exponential stability. It hence is more capable of ensuring stability when the system states are not always available and the phenomenon of time delays occurs. However, no related study has been reported on the adaptive neural quantized control for switched nonlinear large-scale delayed systems by using the output-feedback control in the finite-time tracking under a category of switching signals satisfying the persistent dwell time.

Motivated by the above discussions, this study focuses on the decentralized finite-time neural output feedback quantized control for switched nonlinear large-scale delayed systems. The main technical challenge arises from dealing with quantized input and time delays for switched nonlinear large-scale delayed systems under a suitable switching signal. These challenges are addressed in this article, and the main contributions of this study are summarized as follows:

1. The decentralized finite-time adaptive neural output-feedback quantized tracking control scheme is flexibly designed for the switched nonlinear large-scale delayed systems using the multiple Lyapunov–Krasovskii functions. While the similar control problem has been addressed in References [32, 35], these studies are confined to a class of single-input and single-output nonswitched nonlinear systems. Thus, they cannot be applied to switched nonlinear large-scale delayed systems due to the presence of large-scale time delays and interconnected subsystems.
2. By the nonlinear decomposition technique, quantization errors from input quantized signals have been addressed for each subsystem. Different from the quantized control for the nonswitched nonlinear systems or nondelayed systems in References [32, 39, 40], undesired chattering is effectively prevented for switched nonlinear large-scale delayed systems under a category of switching signals satisfying the persistent dwell time.
3. By designing a switched high-gain quantized state observer to estimate the unmeasured states, the proposed decentralized adaptive output feedback control approach eliminates the restrictive assumption in References [18, 25] that states are available during the control design. Moreover, the stability of the closed-loop system is guaranteed such that the tracking errors can remain in a small domain near the origin in a finite time via the dynamic surface control technique.

The remainder of this study is arranged as follows. The system description is mainly introduced in Section 2. The controller scheme and stability analysis are presented in Section 3. The effectiveness and flexibility of the proposed control strategy are shown in Section 4. The conclusions are finally drawn in Section 5.

2 | System Description

2.1 | Switched Nonlinear Large-Scale Delayed Systems

Consider the following switched nonlinear large-scale delayed systems

$$\dot{x}_{il} = x_{i,l+1} + f_{il\sigma(t)}(x) + h_{il\sigma(t)}(x_\tau) \tag{1a}$$

10991239, 2025, 6, Downloaded from https://onlinelibrary.wiley.com/doi/10.1002/rnc.7765 by HONG KONG POLYTECHNIC UNIVERSITY HU NG HOM, Wiley Online Library on [20/09/2025]. See the Terms and Conditions (https://onlinelibrary.wiley.com/terms-and-conditions) on Wiley Online Library for rules of use; OA articles are governed by the applicable Creative Commons License

$$\dot{x}_{im} = Q(u_{i\sigma(t)}) + f_{im\sigma(t)}(x) + h_{im\sigma(t)}(x_\tau) \tag{1b}$$

$$y_i = x_{i1} \tag{1c}$$

where $l = 1, \ldots, m-1$ and $x_i = [x_{i1}, \ldots, x_{im}]^\top \in \mathbb{R}^m$ is the system state with $x = [x_1^\top, \ldots, x_n^\top]^\top \in \mathbb{R}^{nm}$. The switched systems (1) consist of n interconnected subsystems $\aleph_i$ for $i = 1, \ldots, n$. A switching signal $\sigma(t)$ is defined as $\sigma(t) : [0, \infty) \to \mathbb{M} = \{1, \ldots, \overline{M}\}$ with $\overline{M} \geq 2$ being the number of subsystems. Note that during $t \in [t_k, t_{k+1})$, one gets $\sigma(t) = k \in \mathbb{M}$, where t_k and t_{k+1} are the time instant. During the time interval $\left[t_k, t_{k+1}\right)$, the k-th subsystem is active with the switching time instant t_k. The control input of the k-th subsystem is described by $u_k = [u_{1k}, \ldots, u_{nk}]^\top \in \mathbb{R}^n$. $y = [y_1, \ldots, y_n]^\top \in \mathbb{R}^n$ is the system output. $Q(\cdot)$ is the quantization function to be designed later. For $k \in \mathbb{M}$ and $l = 1, \ldots, m$, $f_{ilk}(\cdot) \in \mathbb{R}$ and $h_{ilk}(\cdot) \in \mathbb{R}$ are the unknown continuous nonlinear functions. For the known constants $\tau > 0$ and $\overline{\tau} > 0$, the delayed state x_τ is defined as $x_\tau = [x_{1\tau}^\top, \ldots, x_{n\tau}^\top]^\top \in \mathbb{R}^{n\times m}$ with $x_{i\tau} = x_i(t - \tau_i(t))$ and $x_{ij\tau} = x_{ij}(t - \tau_i(t))$ for $i = 1, \ldots, n$ and $j = 1, \ldots, n$, where $\tau_i(t)$ is the unknown time-varying delay satisfying $0 < \tau_i(t) \leq \tau$ and $\dot{\tau}_i(t) \leq \overline{\tau} < 1$. In this case, $\Gamma(t_0) = x(t_0) \in \mathbb{R}^{n\times m}$ represents the initial vector at $t_0 \in [-\tau, 0]$.

For given reference signals $y_{ir}(t)$ $(i = 1, \ldots, n)$, the control objective is constructing decentralized finite-time adaptive output-feedback quantized controllers of subsystems for the switched nonlinear large-scale delayed systems based on the multiple Lyapunov–Krasovskii functions such that, for any bounded initial conditions, the following hold:

1. all the closed-loop signals are semi-globally uniformly ultimate bounded under a category of switching signals with the persistent dwell time;
2. the tracking error $y_i - y_{ir}$ $(i = 1, 2, \ldots, n)$ converges to a small domain around the origin in a finite time.

Assumption 1. For any $k \in \mathbb{M}$, the nonlinear functions $f_{ilk}(\cdot)$ and $h_{ilk}(\cdot)$ can satisfy $f_{ilk}^2(x) \leq \sum_{j=1}^n F_{ilj}^2(x_j)$ and $h_{ilk}^2(x_\tau) \leq \sum_{j=1}^n H_{ilj}^2(x_{j\tau})$ with $l = 1, \ldots, m$ and $i = 1, \ldots, n$, where F_{ilj} and H_{ilj} are unknown non-negative smooth functions satisfying $F_{ilj}(0) = 0$ and $H_{ilj}(0) = 0$, respectively.

Assumption 2. The reference signals $y_{ir}(t)$ and their derivatives $\dot{y}_{ir}$ and $\ddot{y}_{ir}$ are continuous and bounded, satisfying $\Omega_{Yi} = \{[y_{ir}, \dot{y}_{ir}, \ddot{y}_{ir}]^\top : y_{ir}^2 + \dot{y}_{ir}^2 + \ddot{y}_{ir}^2 \leq Y_i\}$ with $\overline{Y}_i$ being a positive constant.

Remark 1. Assumption 1 is a general assumption that is used to deal with the nonlinear time-delay terms. In fact, for any continuous function $h_{ilk}(x_{1\tau}, \ldots, x_{n\tau}) : \mathbb{R}^{n\times m} \to \mathbb{R}$, there exist positive smooth functions $H_{il1}(x_{1\tau}), \ldots, H_{iln}(x_{n\tau})$ such that $|h_{ilk}(x_\tau)| \leq \sum_{j=1}^n H_{ilj}(x_{j\tau})$, that is, $h_{ilk}^2(x_\tau) \leq \sum_{j=1}^n H_{ilj}^2(x_{j\tau})$, which can be commonly found such as in References [18, 41]. Assumption 2 is a standard assumption widely employed in the study of adaptive tracking control, both for nonswitched nonlinear systems [5, 40] and for switched nonlinear systems [39, 42].

Lemma 1. (Reference [43]). *Consider a smooth positive-definite function $V(x)$ in a set $\Omega_x \in \mathbb{R}^n$ for the nonlinear system $\dot{x} = f(x, u)$. If positive constant c exists, then $\dot{V}(x) \leq -cV^{w'}(x), t \geq 0$, where $0 < w' < 1$, and the system $\dot{x} = f(x, u)$ is semi-global practically finite-time stable. Besides, $V(x) \equiv 0$ is arrived at the finite time T_x satisfying $T_x \leq V^{1-w'}(x_0)/[c(1 - w')]$, where $V(x_0)$ is the initial value of $V(x)$.*

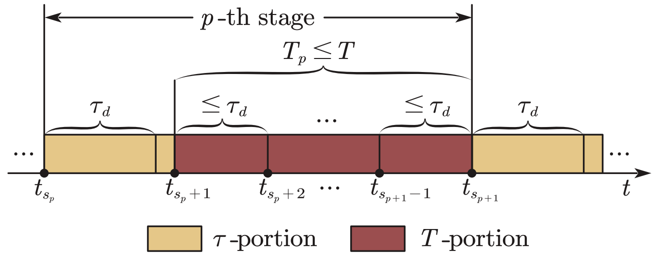

FIGURE 1 | Schematic of the persistent dwell time switching.

2.2 | Persistent Dwell Time Switching

Definition 1. (Reference [20]). Consider the switching sequence produced by a switching signal $\sigma(t)$. τ_d can be denoted as the persistent dwell time when an infinite number of disjoint intervals of length no shorter than a positive constant τ_d exists. Meanwhile, a persistence period T separates the successive intervals from the above disjoint intervals.

In the persistent dwell time switching, the time interval is divided into several stages shown in Figure 1. Each stage consists of the period of persistence T-portion and the running time of the subsystem τ-portion. Denote the switching interval $(t_{s_p}, t_{s_{p+1}})$ as the p-th stage of the PDT switching with a positive integer p. Meanwhile, in the p-th stages, t_{s_p} represents the initial switching moment, while t_{s_p+1} represents the next switching moment after t_{s_p}. Based on $N(t_{s_p+1}, t_{s_{p+1}})$ as the number of switches during $(t_{s_p+1}, t_{s_{p+1}})$ in the T-portion, the running time T_p meets the following condition:

$$T_p = \sum_{i=1}^{N(t_{s_p+1}, t_{s_{p+1}})} T(t_{s_p+i}, t_{s_p+i+1}) \leq T \tag{2}$$

where $T(t_{s_p+i}, t_{s_p+i+1}) = t_{s_p+i+1} - t_{s_p+i}$. In the T-portion, let the switching frequency of the p-th stage be $\hat{f}_p = N(t_{s_p+1}, t_{s_{p+1}})/T_p$. Then, according to Reference [21], the switching frequency $\hat{f}_p$ holds that $\hat{f}_p \leq \hat{f}$, where $\hat{f}$ stands for a known positive parameter. For any interval (t_1, t_2), the number of switchings $N(t_1, t_2)$ holds that

$$N\left(t_1, t_2\right) \leq \left(\frac{t_2 - t_1}{\tau_d + T} + 1\right)(T\hat{f} + 1) \tag{3}$$

2.3 | Neural Networks Approximation

The radial basis function-based neural network is considered as follows:

$$\overline{f}_{NN}(X) = W^\top S(X) \in \mathbb{R} \tag{4}$$

where the weight vector $W \in \mathbb{R}^\ell$ contains ℓ nodes whose number is greater than one, and its basic function vector $S(X) \in$

10991239, 2025, 6, Downloaded from https://onlinelibrary.wiley.com/doi/10.1002/rnc.7765 by HONG KONG POLYTECHNIC UNIVERSITY HU NG HOM, Wiley Online Library on [20/09/2025]. See the Terms and Conditions (https://onlinelibrary.wiley.com/terms-and-conditions) on Wiley Online Library for rules of use; OA articles are governed by the applicable Creative Commons License

$\mathbb{R}^{\ell}$ contains the input vector X. Meanwhile, the $W^{*\top}S(X)$ satisfies

$$\overline{f}(X) = W^{*\top}S(X) + \delta(X) \tag{5}$$

where $X = [x_1, \ldots, x_n]^\top \in \mathbb{R}^n$ and $\delta(X)$ is the error of approximation satisfying $|\delta(X)| \le \delta^*$ with any given positive constant δ^*. In addition, W^* demonstrates an ideal weight vector. Consider $S(X) = [s_1(X), \ldots, s_\ell(X)]^\top \in \mathbb{R}^\ell$ with the Gaussian functions $s_i(X)$ as follows for $i = 1, \ldots, \ell$,

$$s_i(X) = \exp\left[\frac{-\left(X - \vartheta_i\right)^\top\left(X - \vartheta_i\right)}{\imath^2}\right] \tag{6}$$

where $\imath$ is the width and $\vartheta_i = [\vartheta_{i1}, \ldots, \vartheta_{in}]^\top$ is the center. For convenience, $\overline{f}(X)$ is defined as $\overline{f}(X) = W^{*\top}S + \delta$ with

$$W^* = \arg\min_{W\in\mathbb{R}^\ell}\left\{\sup_{X\in\Omega}\left|\overline{f}(X) - \overline{f}_{NN}(X)\right|\right\} \tag{7}$$

3 | Main Results

By employing the multiple Lyapunov–Krasovskii functions, for the switched system (1), this section will develop a decentralized neural output-feedback quantized adaptive control scheme in the constructive design via the backstepping method with the dynamic surface control technique. The analysis of stability will be shown in the resulting closed-loop switched system under the persistent dwell time in finite time.

3.1 | Hysteresis Quantizer Design

The input hysteresis quantizer is considered as follows:

$$Q(u_{ik}) = \begin{cases} u_{i\overline{n}}\mathrm{sgn}(u_{ik}),\ \frac{u_{i\overline{n}}}{1+\rho_i} < |u_{ik}| \le u_{i\overline{n}}, \dot{u}_{ik} < 0, \\ \qquad \text{or } u_{i\overline{n}} < |u_{ik}| \le \frac{u_{i\overline{n}}}{1-\rho_i}, \dot{u}_{ik} > 0; \\ u_{i\overline{n}}(1+\rho_i)\mathrm{sgn}(u_{ik}), u_{i\overline{n}} < |u_{ik}| \le \frac{u_{i\overline{n}}}{1-\rho_i}, \dot{u}_{ik} < 0, \\ \qquad \text{or } \frac{u_{i\overline{n}}}{1-\rho_i} < |u_{ik}| \le \frac{u_{i\overline{n}}(1+\rho_i)}{1-\rho_i}, \dot{u}_{ik} > 0; \\ 0, 0 \le |u_{ik}| < \frac{u_{i,\min}}{1+\rho_i}, \dot{u}_{ik} < 0, \\ \qquad \text{or } \frac{u_{i,\min}}{1+\rho_i} < |u_{ik}| \le u_{i,\min}, \dot{u}_{ik} > 0; \\ Q(u_{ik}(t^-)), \text{otherwise} \end{cases} \tag{8}$$

where u_{ik} is the notation of the system input, $u_{i\overline{n}} = \chi_i^{1-\overline{n}}u_{i,\min}$ ($\overline{n} = 1, 2, \ldots$) and $\rho_i = (1-\chi_i)/(1+\chi_i)$ with $u_{i,\min} > 0$ and $0 < \chi_i < 1$. The quantization function $Q(u_{ik})$ belongs to the set $\Omega_Q = \{0, \pm u_{i\overline{n}}, \pm u_{i\overline{n}}(1+\rho_i), \overline{n} = 1, 2, \ldots, \}$. Here, the constant $u_{i,\min}$ stands for the range of the dead zone for $Q(u_{ik})$, and the constant χ_i represents the measure of quantization density. The schematic of the hysteresis quantizer is depicted in Figure 2.

Since the quantization function $Q(u_{ik})$ from the system input of each subsystem is piecewise continuous, the design of the suitable controllers becomes complex in the backstepping technique. Thus, the following lemma introduces a nonlinear decomposition technique for the quantization function.

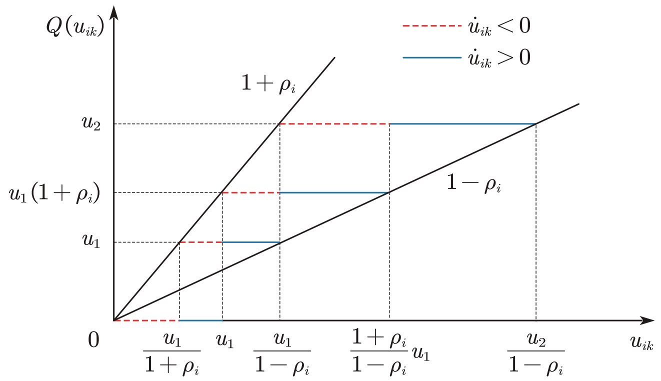

FIGURE 2 | Schematic of the hysteresis quantizer.

Lemma 2. (Reference [30]). *The hysteretic quantizer $Q(u_{ik})$ can be decomposed as follows*:

$$Q(u_{ik}) = G(u_{ik})u_{ik}(t) + D(t) \tag{9}$$

where $G(u_{ik})$ and $D(t)$ satisfy

$$1 - \rho_i \le G(u_{ik}) \le 1 + \rho_i,\ |D(t)| \le u_{i,\min} \tag{10}$$

3.2 | Switched High-Gain Quantized State Observer Design

To estimate the unavailable states, a switched high-gain quantized state observer is considered as

$$\dot{\hat{x}}_{il} = \hat{x}_{i,l+1} + L_{il\sigma(t)}(y_i - \hat{x}_{i1}) \tag{11a}$$

$$\dot{\hat{x}}_{im} = Q(u_{i\sigma(t)}) + L_{im\sigma(t)}(y_i - \hat{x}_{i1}) \tag{11b}$$

where $l = 1, \ldots, m-1$, $\sigma(t)$ is the same switching signal as described in the switched system (1), and $\hat{x}_{il}$ is the estimate of the system state x_{il} for $l = 1, 2, \ldots, m$. L_{ilk} denotes positive constants to be designed such that the matrix A_{ik} is Hurwitz, where $A_{ik} = \bar{A} - L_{ik}C$ with $\bar{A} = [0, \bar{A}_0] \in \mathbb{R}^{m\times m}$, $\bar{A}_0 = [I_{m-1}, 0]^\top \in \mathbb{R}^{m\times(m-1)}$, $L_{ik} = [L_{i1k}, \ldots, L_{imk}]^\top \in \mathbb{R}^m$, $C = [1, 0, \ldots, 0] \in \mathbb{R}^{1\times m}$, and $I_{m-1} \in \mathbb{R}^{(m-1)\times(m-1)}$ is an identity matrix for $k \in \mathbb{M}$ and $l = 1, 2, \ldots, m$.

In other words, for definite symmetric matrices $B_{ik} > 0$, the symmetric definite matrix $P_{ik} > 0$ exists and satisfies

$$A_{ik}^\top P_{ik} + P_{ik}A_{ik} = -B_{ik} \tag{12}$$

Denote the state vector of the observer as $\hat{x} = [\hat{x}_1^\top, \ldots, \hat{x}_n^\top]^\top \in \mathbb{R}^{nm}$ with $\hat{x}_i = [\hat{x}_{i1}, \ldots, \hat{x}_{im}]^\top$ for $i = 1, \ldots, n$. Let the error of the state observer be

$$\varepsilon_i = [\varepsilon_{i1}, \ldots, \varepsilon_{im}]^\top = x_i - \hat{x}_i \in \mathbb{R}^m \tag{13}$$

To proceed with, combining (1) with (11), one gets

$$\dot{\varepsilon}_i = A_{ik}\varepsilon_i + f_{ik}(x) + h_{ik}(x_\tau) \tag{14}$$

10991239, 2025, 6, Downloaded from https://onlinelibrary.wiley.com/doi/10.1002/rnc.7765 by HONG KONG POLYTECHNIC UNIVERSITY HU NG HOM, Wiley Online Library on [20/09/2025]. See the Terms and Conditions (https://onlinelibrary.wiley.com/terms-and-conditions) on Wiley Online Library for rules of use; OA articles are governed by the applicable Creative Commons License

where $k \in \mathbb{M}$, $f_{i,k} = [f_{i1k}, \dots, f_{imk}]^\top \in \mathbb{R}^m$ and $h_{i,k} = [h_{i1k}, \dots, h_{imk}]^\top \in \mathbb{R}^m$. As a matter of convenience, the unknown ideal values are expressed as

$$\theta_{il}^* = \max\{\|W_{ilk}^*\|,\ k \in \mathbb{M}\} \tag{15}$$

where $l = 0, 1, \dots, m$, W_{ilk}^* stands for the ideal constant weight vector. Meanwhile, $\tilde{\theta}_{il}$ is the estimation error satisfying $\tilde{\theta}_{il} = \theta_{il}^* - \hat{\theta}_{il}$, and $\hat{\theta}_{il}$ is the estimation of θ_{il}^*.

For the observer error system (14), let the Lyapunov function candidate be

$$V_{i0k} = \varrho_i \varepsilon_i^\top P_{ik} \varepsilon_i,\ i = 1, \dots, n,\ k \in \mathbb{M} \tag{16}$$

where ϱ_i is a positive parameter. By using (12) and (14), one gets $\dot{V}_{i0k}$ satisfied by

$$\dot{V}_{i0k} = 2\varrho_i \varepsilon_i^\top P_{ik}[f_{ik}(x) + h_{ik}(x_\tau)] + \varrho_i \varepsilon_i^\top (A_{ik}^\top P_{ik} + P_{ik} A_{ik})\varepsilon_i \tag{17}$$

In what follows, the inequalities are determined by the definition of Young's inequality

$$2\varrho_i \varepsilon_i^\top P_{ik} f_{ik}(x) \le \varrho_i r_{i0} e^{\beta\tau} \|\varepsilon_i\|^2 + \frac{\varrho_i e^{-\beta\tau}}{r_{i0}} \|P_{ik}\|^2 \sum_{l=1}^{m} \sum_{j=1}^{n} F_{ilj}^2(x_j) \tag{18}$$

$$2\varrho_i \varepsilon_i^\top P_{ik} h_{ik}(x_\tau) \le \varrho_i r_{i0} e^{\beta\tau} \|\varepsilon_i\|^2 + \frac{\varrho_i e^{-\beta\tau}}{r_{i0}} \|P_{ik}\|^2 \sum_{l=1}^{m} \sum_{j=1}^{n} H_{ilj}^2(x_{j\tau}) \tag{19}$$

where β and r_{i0} are the positive parameters. Suppose that the unknown continuous function is $\overline{f}_{i0k}(X_{i0})$. Furthermore, combining (5) and (15) yields

$$\overline{f}_{i0k}(X_{i0}) \le \|W_{i0k}^{*\top} S_{i0}(X_{i0})\| + |\delta_{i0k}| \le \theta_{i0}^* + \delta_{i0}^* \tag{20}$$

Then, substituting (12) and (18–20) into (17), one gets

$$\begin{aligned} \dot{V}_{i0k} \le& -\varrho_i(\underline{\lambda}(B_{ik}) - 2r_{i0}e^{\beta\tau})\|\varepsilon_i\|^2 + \Theta_{i0k} - \overline{f}_{i0k}(X_0) \\ &+ \frac{\varrho_i e^{-\beta\tau}}{r_{i0}} \|P_{ik}\|^2 \sum_{l=1}^{m} \sum_{j=1}^{n} (F_{ilj}^2(x_j) + H_{ilj}^2(x_{j\tau})) \end{aligned} \tag{21}$$

where $\underline{\lambda}(B_{ik})$ represents the smallest eigenvalue of the matrix B_{ik}, and Θ_{i0k} is an unknown constant with $\Theta_{i0k} = \theta_{i0}^* + \delta_{i0}^*$.

Remark 2. A quantizer is referred to as a sector-bounded quantizer if the quantization error satisfies the sector-bounded condition. It is noted in Reference [44] that, several typical quantizers, such as the logarithmic quantizer and the hysteresis quantizer, fall within the framework of sector-bounded quantizers. Compared to the logarithmic quantizer, the hysteresis quantizer offers a broader range of applications. It can maintain its output value for a period before changing, effectively avoiding the chattering phenomenon. This characteristic is particularly advantageous in switched systems requiring stable and consistent signal processing for the state observer design.

3.3 | Adaptive Output-Feedback Quantized Controllers Design

The common changes of the coordinate for each switched subsystem are designed as follows:

$$z_{i1} = x_{i1} - y_{ir} \tag{22a}$$

$$z_{il} = \hat{x}_{il} - \xi_{il} \tag{22b}$$

$$\eta_{il} = \xi_{il} - \alpha_{i,l-1},\ l = 2, \dots, m \tag{22c}$$

where z_{il} denotes the error surface for $l = 1, \dots, m$. $\alpha_{i,l-1}$ and ξ_{il} are the input and output for a first-order filter $q_{il}\dot{\xi}_{il} + \xi_{il} = \alpha_{i,l-1}$ with a time constant $q_{il} > 0$ for $l = 2, \dots, m$, respectively. η_{il} is the output error for the first-order filter with $\eta_{i1} = 0$. From (1), (11), and (13), the dynamics of (22) are given by

$$\dot{z}_{i1} = \hat{x}_{i2} + \varepsilon_{i2} + f_{i1k}(x) + h_{i1k}(x_\tau) - \dot{y}_{ir} \tag{23a}$$

$$\dot{z}_{il} = \hat{x}_{i,l+1} + L_{ilk}(y_i - \hat{x}_{i1}) - \dot{\xi}_{il} \tag{23b}$$

where $\hat{x}_{i,m+1} = Q(u_{ik})$ for $k \in \mathbb{M}$ and $l = 2, 3, \dots, m$. According to the definition of η_{il} in (22c), one gets

$$\dot{\eta}_{il} = \dot{\xi}_{il} - \dot{\alpha}_{i,l-1} = -\frac{\eta_{il}}{q_{il}} + \Phi_{il}(\cdot) \tag{24}$$

where $\xi_{il}(0) = \alpha_{i,l-1}(0)$ and $\Phi_{il}(\cdot)$ is a continuous function with respect to the vector X_{il} to be determined later. The detailed design process of the control scheme is shown in the following steps.

Initial Step: Construct the following Lyapunov function as

$$V_{i1k} = V_{i0k} + \frac{1}{2} z_{i1}^2 + \frac{1}{2\ell_{i1}} \tilde{\theta}_{i1}^2,\ k \in \mathbb{M} \tag{25}$$

where ℓ_{i1} is a positive constant. To proceed with, based on (1), (13), (22–25), one gets

$$\begin{aligned} \dot{V}_{i1k} =& z_{i1}[z_{i2} + \eta_{i2} + \alpha_{i1} + \varepsilon_{i2} + f_{i1k}(x) + h_{i1k}(x_\tau) - \dot{y}_{ir}] \\ &+ \dot{V}_{i0k} - \frac{1}{\ell_{i1}} \tilde{\theta}_{i1} \dot{\hat{\theta}}_{i1} \end{aligned} \tag{26}$$

By utilizing Young's inequality, one has

$$z_{i1}\varepsilon_{i2} \le \frac{e^{-\beta\tau}}{4\varrho_i r_{i0}} z_{i1}^2 + \varrho_i r_{i0} e^{\beta\tau} \|\varepsilon_i\|^2 \tag{27}$$

$$z_{i1} f_{i1k}(x) \le \frac{r_{i1} e^{\beta\tau}}{2} z_{i1}^2 + \frac{e^{-\beta\tau}}{2r_{i1}} \sum_{j=1}^{n} F_{i1j}^2(x_j) \tag{28}$$

$$z_{i1} h_{i1k}(x_\tau) \le \frac{r_{i1} e^{\beta\tau}}{2} z_{i1}^2 + \frac{e^{-\beta\tau}}{2r_{i1}} \sum_{j=1}^{n} H_{i1j}^2(x_{j\tau}) \tag{29}$$

where r_{i1} is a positive parameter. Then, $\overline{f}_{i1k}(X_{i1}) = [e^{-\beta\tau}/(4\varrho_i r_{i0}) + r_{i1}e^{\beta\tau}]z_{i1} - \dot{y}_{ir}$ is denoted as the uncertain continuous

10991239, 2025, 6, Downloaded from https://onlinelibrary.wiley.com/doi/10.1002/rnc.7765 by HONG KONG POLYTECHNIC UNIVERSITY HU NG HOM, Wiley Online Library on [20/09/2025]. See the Terms and Conditions (https://onlinelibrary.wiley.com/terms-and-conditions) on Wiley Online Library for rules of use; OA articles are governed by the applicable Creative Commons License

function with $X_{i1} = [x_{i1}, y_{ir}, \dot{y}_{ir}]^\top$. Based on (5–7), it can be approximated by a neural network satisfying

$$\overline{f}_{i1k}(X_{i1}) = W_{i1k}^{*\top} S_{i1} + \delta_{i1k} \tag{30}$$

where δ_{i1k} is the approximation error $|\delta_{i1k}| < \delta_{i1}^*$ and δ_{i1}^* is a positive constant. Based on (15) and (30), one gets

$$\begin{aligned} z_{i1}\overline{f}_{i1k}(X_{i1}) &= z_{i1} W_{i1k}^{*\top} S_{i1} + z_{i1}\delta_{i1k} \\ &\le \frac{1}{2a_{i1}^2} z_{i1}^2 \theta_{i1}^* S_{i1}^\top S_{i1} + \frac{1}{2} a_{i1}^2 + \frac{1}{2} z_{i1}^2 + \frac{1}{2}\delta_{i1}^{*2} \end{aligned} \tag{31}$$

where a_{i1} is a positive parameter. Meanwhile, the finite-time virtual controller input α_{i1} and the adaptive law $\dot{\hat{\theta}}_{i1}$ are determined as

$$\alpha_{i1} = -\frac{1}{2a_{i1}^2} z_{i1}\hat{\theta}_{i1} S_{i1}^\top S_{i1} - \frac{1}{2} z_{i1} - c_{i1} z_{i1} - \overline{c}_{i1} |z_{i1}|^{\omega} \mathrm{sgn}(z_{i1}) \tag{32}$$

$$\dot{\hat{\theta}}_{i1} = \frac{\ell_{i1}}{2a_{i1}^2} z_{i1}^2 S_{i1}^\top S_{i1} - \gamma_{i1}\hat{\theta}_{i1} \tag{33}$$

where c_{i1}, $\overline{c}_{i1}$, and γ_{i1} are some positive parameters.

Substituting (27–33) into (26) results in

$$\begin{aligned} \dot{V}_{i1k} \le & -\varrho_i(\underline{\lambda}(B_{ik}) - 3r_{i0}e^{\beta\tau})\|\varepsilon_i\|^2 + \frac{\gamma_{i1}}{\ell_{i1}}\tilde{\theta}_{i1}\hat{\theta}_{i1} + z_{i1}\eta_{i2} \\ & - c_{i1}z_{i1}^2 - \overline{c}_{i1}|z_{i1}|^{\omega+1} + z_{i1}z_{i2} + \Theta_{i1k} - \overline{f}_{i0k}(X_0) \\ & + \frac{\varrho_i e^{-\beta\tau}}{r_0}\|P_{ik}\|^2 \sum_{l=1}^{m}\sum_{j=1}^{n}(F_{ilj}^2(x_j) + H_{ilj}^2(x_{j\tau})) \\ & + \frac{e^{-\beta\tau}}{2r_{i1}}\sum_{j=1}^{n}(F_{i1j}^2(x_j) + H_{i1j}^2(x_{j\tau})) \end{aligned} \tag{34}$$

where $\Theta_{i1k} = \Theta_{i0k} + a_{i1}^2/2 + \delta_{i1}^{*2}/2$.

Inductive Step ($2 \le l \le m-1$): The Lyapunov function can be constructed by

$$V_{ilk} = V_{i,l-1,k} + \frac{1}{2}z_{il}^2 + \frac{1}{2\ell_{il}}\tilde{\theta}_{il}^2 + \frac{1}{2}\eta_{il}^2 \tag{35}$$

where ℓ_{il} is a positive constant. Furthermore, it is deduced that

$$\begin{aligned} \dot{V}_{ilk} = & z_{il}[z_{i,l+1} + \eta_{i,l+1} + \alpha_{i,l} + L_{ilk}\varepsilon_{i1} - \dot{\xi}_{il}] + \dot{V}_{i,l-1,k} \\ & - \frac{1}{\ell_{il}}\tilde{\theta}_{il}\dot{\hat{\theta}}_{il} - \left(\frac{\eta_{il}^2}{q_{il}} - \Phi_{il}(\cdot)\eta_{il}\right) \end{aligned} \tag{36}$$

By utilizing Young's inequality, one gets

$$z_{il}L_{ilk}\varepsilon_{i1} \le \frac{e^{-\beta\tau}}{4\varrho_i r_{i0}}L_{ilk}^2 z_{il}^2 + \varrho_i r_{i0}e^{\beta\tau}\|\varepsilon_i\|^2 \tag{37}$$

where r_{il} is a positive parameter. Similar to the initial step, the uncertain functions are considered as $\overline{f}_{ilk}(X_{il}) = e^{-\beta\tau}L_{ilk}^2 z_{il}/(4\varrho_i r_{i0}) + z_{i,l-1}$ with $X_{il} = [x_{i1}, y_{ir}, \dot{y}_{ir}, \ddot{y}_{ir}, \hat{\theta}_{i1}, \ldots, \hat{\theta}_{i,l-1}, \hat{x}_{i1}, \ldots, \hat{x}_{il}]^\top$. Based on (5–7), the uncertain functions $\overline{f}_{ilk}(X_{il})$ can also be approximated by a neural network satisfying

$$\overline{f}_{ilk}(X_{il}) = W_{ilk}^{*\top} S_{il} + \delta_{ilk} \tag{38}$$

where the error of approximation δ_{ilk} is satisfied by $|\delta_{ilk}| < \delta_{il}^*$ with a positive parameter δ_{il}^*. Based on Young's inequality, (15), and (38), one has

$$\begin{aligned} z_{il}\overline{f}_{ilk}(X_{il}) &= z_{il}W_{ilk}^{*\top}S_{il} + z_{il}\delta_{ilk} \\ &\le \frac{1}{2a_{il}^2} z_{il}^2\theta_{il}^* S_{il}^\top S_{il} + \frac{1}{2}a_{il}^2 + \frac{1}{2}z_{il}^2 + \frac{1}{2}\delta_{il}^{*2} \end{aligned} \tag{39}$$

where a_{il} is the positive designed parameter. Meanwhile, the finite-time virtual controller input α_{il} and the adaptive laws $\dot{\hat{\theta}}_{il}$ can be considered as

$$\alpha_{il} = -\frac{1}{2a_{il}^2} z_{il}\hat{\theta}_{il} S_{il}^\top S_{il} - \frac{1}{2}z_{il} - c_{il}z_{il} - \overline{c}_{il}|z_{il}|^{\omega}\mathrm{sgn}(z_{il}) + \dot{\xi}_{il} \tag{40}$$

$$\dot{\hat{\theta}}_{il} = \frac{\ell_{il}}{2a_{il}^2} z_{il}^2 S_{il}^\top S_{il} - \gamma_{il}\hat{\theta}_{il} \tag{41}$$

where c_{il}, $\overline{c}_{il}$, and γ_{il} are positive parameters. Substituting (38–41) into (36) yields

$$\begin{aligned} \dot{V}_{ilk} \le & -\varrho_i[\underline{\lambda}(B_{ik}) - (2+l)r_{i0}e^{\beta\tau}]\|\varepsilon_i\|^2 + z_{il}z_{i,l+1} \\ & + \Theta_{ilk} + \frac{\varrho_i e^{-\beta\tau}}{r_0}\|P_{ik}\|^2\sum_{l=1}^{m}\sum_{j=1}^{n}(F_{ilj}^2(x_j) + H_{ilj}^2(x_{j\tau})) \\ & + \frac{e^{-\beta\tau}}{2r_{i1}}\sum_{j=1}^{n}(F_{i1j}^2(x_j) + H_{i1j}^2(x_{j\tau})) - \overline{f}_{i0k}(X_0) \\ & + \sum_{j=1}^{l}\left(\frac{\gamma_{ij}}{\ell_{ij}}\tilde{\theta}_{ij}\hat{\theta}_{ij} - c_{ij}z_{ij}^2 - \overline{c}_{ij}|z_{ij}|^{\omega+1}\right) \\ & + \sum_{j=1}^{l-1}z_{ij}\eta_{i,j+1} - \sum_{j=2}^{l}\left(\frac{\eta_{ij}^2}{q_{ij}} - \Phi_{ij}(\cdot)\eta_{ij}\right) \end{aligned} \tag{42}$$

where $\Theta_{ilk} = \Theta_{i,l-1,k} + a_{il}^2/2 + \delta_{il}^{*2}/2$.

Step m: Let the Lyapunov function candidate be

$$V_{imk} = V_{i,m-1,k} + \frac{1}{2}z_{im}^2 + \frac{1}{2\ell_{im}}\tilde{\theta}_{im}^2 + \frac{1}{2}\eta_{im}^2 \tag{43}$$

where ℓ_{im} is a positive constant. Also, it is deduced that

$$\begin{aligned} \dot{V}_{imk} = & z_{im}[G(u_{ik})u_{ik} + D(t) + L_{imk}\varepsilon_{i1} - \dot{\xi}_{il}] + \dot{V}_{i,m-1,k} \\ & - \frac{1}{\ell_{im}}\tilde{\theta}_{im}\dot{\hat{\theta}}_{im} - \left(\frac{\eta_{im}^2}{q_{im}} - \Phi_{im}(\cdot)\eta_{im}\right) \end{aligned} \tag{44}$$

Utilizing Young's inequality induces

$$z_{im}L_{imk}\varepsilon_{i1} \le \frac{e^{-\beta\tau}}{4\varrho_i r_{i0}}L_{imk}^2 z_{im}^2 + \varrho_i r_{i0}e^{\beta\tau}\|\varepsilon_i\|^2 \tag{45}$$

$$z_{im}D(t) \le \frac{1}{4}z_{im}^2 + u_{ik,\min}^2 \tag{46}$$

10991239, 2025, 6, Downloaded from https://onlinelibrary.wiley.com/doi/10.1002/rnc.7765 by HONG KONG POLYTECHNIC UNIVERSITY HU NG HOM, Wiley Online Library on [20/09/2025]. See the Terms and Conditions (https://onlinelibrary.wiley.com/terms-and-conditions) on Wiley Online Library for rules of use; OA articles are governed by the applicable Creative Commons License

where r_{im} is a positive parameter and $u^2_{ik,\min}$ is the same as the definition of $\epsilon_{i,\min}$. To proceed with, $\overline{f}_{imk}(X_{im}) = e^{-\beta\tau}L^2_{imk}z_{im}/(4\varrho_i r_{i0}) + z_{i,m-1}$ with $X_{im} = [x_{i1}, y_{ir}, \dot{y}_{ir}, \ddot{y}_{ir}, \hat{\theta}_{i1}, \dots, \hat{\theta}_{i,m-1}, \hat{x}_{i1}, \dots, \hat{x}_{im}]^\top$. Based on (5–7), the neural network approximation is given by

$$\overline{f}_{imk}(X_{il}) = W^{*\top}_{imk}S_{im} + \delta_{imk} \tag{47}$$

where δ_{imk} is the error of approximation and a positive constant δ^*_{im} is satisfied by $|\delta_{imk}| < \delta^*_{im}$. By using (15), (47), and Young's inequality, one has

$$\begin{aligned} z_{im}\overline{f}_{imk}(X_{im}) &= z_{im}W^{*\top}_{imk}S_{im} + z_{im}\delta_{imk} \\ &\le \frac{1}{2a^2_{im}}z^2_{im}\theta^*_{im}S^\top_{im}S_{im} + \frac{1}{2}a^2_{im} + \frac{1}{4}z^2_{im} + \delta^{*2}_{im} \end{aligned} \tag{48}$$

where a_{im} is a positive parameter. Then, the finite-time actual controller input u_{ik} and the adaptive laws $\dot{\hat{\theta}}_{im}$ are constructed as

$$\begin{aligned} u_{ik} = &-\frac{1}{1-\rho_i}\left[\frac{1}{2a^2_{im}}z_{im}\hat{\theta}_{im}S^\top_{im}S_{im} + \frac{1}{2}z_{im} + c_{imk}z_{im}\right. \\ &\left. + \overline{c}_{im}|z_{im}|^{w}\mathrm{sgn}(z_{im}) - \dot{\xi}_{im}\right] \end{aligned} \tag{49}$$

$$\dot{\hat{\theta}}_{im} = \frac{\ell_{im}}{2a^2_{im}}z^2_{im}S^\top_{im}S_{im} - \gamma_{im}\hat{\theta}_{im} \tag{50}$$

where c_{imk}, $\overline{c}_{imk}$, and γ_{im} are positive parameters. Then, based on Lemma 2, (44–50) result in

$$\begin{aligned} \dot{V}_{imk} \le &-\varrho_i[\underline{\lambda}(B_{ik}) - (2+m)r_{i0}e^{\beta\tau}]\|\varepsilon_i\|^2 + \Theta_{imk} \\ &+ \frac{\varrho_i e^{-\beta\tau}}{r_0}\|P_{ik}\|^2\sum_{l=1}^{m}\sum_{j=1}^{n}(F^2_{ilj}(x_j) + H^2_{ilj}(x_{j\tau})) \\ &+ \frac{e^{-\beta\tau}}{2r_{i1}}\sum_{j=1}^{n}(F^2_{i1j}(x_j) + H^2_{i1j}(x_{j\tau})) - \overline{f}_{i0k}(X_0) \\ &+ \sum_{j=1}^{m}\left(\frac{\gamma_{ij}}{\ell_{ij}}\tilde{\theta}_{ij}\hat{\theta}_{ij} - c_{ij}z^2_{ij} - \overline{c}_{ij}|z_{ij}|^{w+1}\right) \\ &+ \sum_{j=1}^{m-1}z_{ij}\eta_{i,j+1} - \sum_{j=2}^{m}\left(\frac{\eta^2_{ij}}{q_{ij}} - \Phi_{ij}(\cdot)\eta_{ij}\right) \end{aligned} \tag{51}$$

where $c_{im} = \max\{c_{imk},\ k \in \mathbb{M}\}$ and $\Theta_{imk} = \Theta_{imk} + u^2_{ik,\min} + a^2_{im}/2 + \delta^{*2}_{im}$.

3.4 | Stability Analysis

First of all, for notational convenience, define

$$\begin{aligned} \mu = \min_{k\in\mathbb{M}}\Bigg\{&\frac{\varrho_i[\underline{\lambda}(B_{ik}) - (2+m)r_{i0}e^{\beta\tau}]}{\overline{\lambda}(P_{ik})}, 2c_{ij} - 1, \gamma_{ij}, \beta, \\ &\frac{2}{q_{ij}} - \overline{\Phi}_{ij} - 1, i = 1, \dots, n,\ j = 1, \dots, m\Bigg\} \end{aligned} \tag{52}$$

$$\upsilon = \max\left\{\frac{\overline{\lambda}(P_{ik})}{\underline{\lambda}(P_{ip})}, k, p \in \mathbb{M},\ i = 1, \dots, n\right\} \tag{53}$$

where $\overline{\lambda}(P_{ik})$ ($\underline{\lambda}(P_{ik})$) refers to the largest (smallest) eigenvalue of the matrix P_{ik}, respectively. Obviously, the inequalities $\varrho_i[\underline{\lambda}(B_{ik}) - (3+m)r_{i0}e^{\beta\tau}] > 0$, $i = 1, \dots, n$, $j = 1, \dots, m$, $k \in \mathbb{M}$ holds by suitably selecting B_{ik}, ϱ_i, r_{i0} and β. Then, $\mu > 0$ and $\upsilon \ge 1$ are the two known parameters.

Theorem 1. *Consider the switched nonlinear large-scale delayed system* (1) *satisfying Assumptions 1 and 2. If the decentralized adaptive output feedback quantized controllers* (49) *are designed with the switched state observer* (11)*, the finite-time virtual controllers* (32)*,* (40)*, and the adaptive laws* (33)*,* (41)*,* (50)*, then the following results hold*:

1. *all signals of the closed-loop system are semi-globally uniformly ultimate bounded under a category of switching signals with the persistent dwell time satisfying* $(\tau_d + T)/(T\hat{f} + 1) \ge (\ln \upsilon)/\mu$;
2. *the tracking error* $y_i - y_{ir}$ $(i = 1, \dots, n)$ *converges to a small domain near the origin in finite time* T_z.

Proof. The proof consists of two parts to analyze the boundedness of all signals in the closed-loop system.

1. Based on (16), (25), (35), and (43), the following multiple Lyapunov–Krasovskii functions are designed as

$$V_k(X) = \sum_{i=1}^{n}(V_{imk}(X_i) + V_{iLK}),\ k \in \mathbb{M} \tag{54}$$

where $X = [X^\top_1, \dots, X^\top_n]^\top$, $X_i = [\varepsilon^\top_i, z_{i1}, \dots, z_{im}, \tilde{\theta}_{i1}, \dots, \tilde{\theta}_{im}, \eta_{i1}, \dots, \eta_{im}]^\top$, and $V_{iLK} = \frac{e^{-\beta t}}{1-\overline{\tau}}\sum_{j=1}^{n}\int_{t-\tau_j(t)}^{t}e^{\beta s}\nu_j(x_j(s))ds$ with $\nu_j(x_j) = \frac{\varrho_i}{r_0}\|P_{ik}\|^2\sum_{l=1}^{m}H^2_{ilj}(x_j) + \frac{1}{2r_{i1}}H^2_{i1j}(x_j)$. In addition, it induces

$$\begin{aligned} \dot{V}_k \le \sum_{i=1}^{n}\Bigg\{ &-\varrho_i[\underline{\lambda}(B_{ik}) - (2+m)r_{i0}e^{\beta\tau}]\|\varepsilon_i\|^2 + \Theta_{imk} \\ &+ \frac{\varrho_i e^{-\beta\tau}}{r_0}\|P_{ik}\|^2\sum_{l=1}^{m}\sum_{j=1}^{n}F^2_{ilj}(x_j) - \beta V_{iLK} \\ &+ \frac{e^{-\beta\tau}}{2r_{i1}}\sum_{j=1}^{n}F^2_{i1j}(x_j) + \sum_{j=1}^{n}\frac{1}{1-\overline{\tau}}\nu_j(x_j) - \overline{f}_{i0k}(X_0) \\ &+ \sum_{j=1}^{m}\left(\frac{\gamma_{ij}}{\ell_{ij}}\tilde{\theta}_{ij}\hat{\theta}_{ij} - c_{ij}z^2_{ij} - \overline{c}_{ij}|z_{ij}|^{w+1}\right) \\ &+ \sum_{j=1}^{m-1}z_{ij}\eta_{i,j+1} - \sum_{j=2}^{m}\left(\frac{\eta^2_{ij}}{q_{ij}} - \Phi_{ij}(\cdot)\eta_{ij}\right)\Bigg\} \end{aligned} \tag{55}$$

Then, the function $\overline{f}_{i0k}(X_0)$, $k \in \mathbb{M}$ can be determined as

$$\begin{aligned} \overline{f}_{i0k}(X_0) = &\frac{\varrho_i e^{-\beta\tau}}{r_0}\|P_{ik}\|^2\sum_{l=1}^{m}F^2_{ilj}(x_j) \\ &+ \frac{e^{-\beta\tau}}{2r_{i1}}F^2_{i1j}(x_j) + \frac{1}{1-\overline{\tau}}\nu_j(x_j) \end{aligned} \tag{56}$$

Furthermore, the terms $\frac{\gamma_{ij}}{\ell_{ij}}\tilde{\theta}_{ij}\hat{\theta}_{ij}$, $z_{ij}\eta_{i,j+1}$ and $\Phi_{ij}(\cdot)\eta_{ij}$ from (55) satisfy

$$\frac{\gamma_{ij}}{\ell_{ij}}\tilde{\theta}_{ij}\hat{\theta}_{ij} \le \frac{\gamma_{ij}}{2\ell_{ij}}\theta^{*2}_{ij} - \frac{\gamma_{ij}}{2\ell_{ij}}\tilde{\theta}^2_{ij} \tag{57}$$

10991239, 2025, 6, Downloaded from https://onlinelibrary.wiley.com/doi/10.1002/rnc.7765 by HONG KONG POLYTECHNIC UNIVERSITY HU NG HOM, Wiley Online Library on [20/09/2025]. See the Terms and Conditions (https://onlinelibrary.wiley.com/terms-and-conditions) on Wiley Online Library for rules of use; OA articles are governed by the applicable Creative Commons License

$$z_{ij}\eta_{i,j+1} \leq \frac{1}{2}z_{ij}^2 + \frac{1}{2}\eta_{i,j+1}^2 \tag{58}$$

$$|\Phi_{ij}(\cdot)\eta_{ij}| \leq \frac{1}{2}\Phi_{ij}^2(\cdot)\eta_{ij}^2 + \frac{1}{2} \tag{59}$$

where $\hat{\theta}_{ij} = \theta_{ij}^* - \tilde{\theta}_{ij}$. Inspired by References [27, 42], for any positive constants $Y_i > 0$ and $\overline{V}_i$, since the sets $\Omega_{Yi} = \{[y_{ir}, \dot{y}_{ir}, \ddot{y}_{ir}]^\top : y_{ir}^2 + \dot{y}_{ir}^2 + \ddot{y}_{ir}^2 \leq Y_i\}$ and $\Omega_{\overline{V}i} = \{V_{imk}(X_i) + V_{iLK} \leq \overline{V}_i\}$ for $i = 1, \dots, n$, are compact sets, $\Omega_{Yi} \times \Omega_{\overline{V}i}$ is also a compact set. Thus, $|\Phi_{ij}(\cdot)|$ has an upper bound $\overline{\Phi}_{ij}$ on the compact set $\Omega_{Yi} \times \Omega_{\overline{V}i}$ because of a continuous function $\Phi_{ij}(\cdot)$. According to (55–59), one has

$$\begin{aligned}
\dot{V}_k \leq \sum_{i=1}^{n} \Big\{ & -\varrho_i[\underline{\lambda}(B_{ik}) - (2+m)r_{i0}e^{\beta\tau}]\|\varepsilon_i\|^2 \\
& - \beta V_{iLK} - \sum_{j=2}^{m}\left(\frac{1}{q_{ij}} - \frac{\overline{\Phi}_{ij}}{2} - \frac{1}{2}\right)\eta_{ij}^2 - \sum_{j=1}^{m}\overline{c}_{ij}|z_{ij}|^{w+1} \\
& - \sum_{j=1}^{m}\frac{\gamma_{ij}}{2\ell_{ij}}\tilde{\theta}_{ij}^2 - \sum_{j=1}^{m}\left(c_{ij} - \frac{1}{2}\right)z_{ij}^2 + \Theta_i \Big\}
\end{aligned} \tag{60}$$

where $\Theta_i = \sum_{i=1}^{n}(\Theta_{imk} + \sum_{j=1}^{m}\gamma_{ij}\theta_{ij}^{*2}/(2\ell_{ij})) + (m-1)/2$. In terms of (52), it is clear that

$$\dot{V}_k \leq -\mu V_k + \Theta \tag{61}$$

where $\Theta = \sum_{i=1}^{n}\Theta_i$. It is observed that if the function $\underline{\kappa}(\cdot) \in \mathcal{K}_\infty$ exists, the following inequality holds:

$$\begin{aligned}
V_k(X(t)) &\geq \sum_{i=1}^{n}\left[\varrho_i\varepsilon_i^\top P_{ik}\varepsilon_i + \sum_{j=1}^{m}\left(\frac{1}{2}z_{ij}^2 + \frac{1}{2\ell_{ij}}\tilde{\theta}_{ij}^2 + \frac{1}{2}\eta_{ij}^2\right)\right] \\
&\geq \underline{\kappa}(\|X(t)\|)
\end{aligned} \tag{62}$$

Moreover, it can be verified from (54) that

$$\begin{aligned}
V_{iLK} &\leq \frac{e^{-\beta t}}{1-\overline{\tau}}\sum_{j=1}^{n}\int_{-\tau_j(t)}^{0} e^{\beta(t+s)}v_j(x_j(t+s))d(t+s) \\
&\leq \frac{e^{-\beta t}}{1-\overline{\tau}}\sum_{j=1}^{n}\sup_{-\tau_j(t)<s<0}\tau_j(t)e^{\beta(t+s)}v_j(x_j(t+s))
\end{aligned} \tag{63}$$

Meanwhile, concerned with a function $\overline{\kappa}(\cdot) \in \mathcal{K}_\infty$, one gets

$$\begin{aligned}
& V_k(X(t)) \\
& \leq \sup_{-\tau_j(t)\leq s\leq 0}\sum_{i=1}^{n}\Big[\varrho_i\varepsilon_i(t+s)^\top P_{ik}\varepsilon_i(t+s) \\
& \quad + \sum_{j=1}^{m}\left(\frac{1}{2}z_{ij}^2(t+s) + \frac{1}{2\ell_{ij}}\tilde{\theta}_{ij}^2(t+s) + \frac{1}{2}\eta_{ij}^2(t+s)\right) + V_{iLK}\Big] \\
& \leq \overline{\kappa}(\sup_{-\tau\leq s\leq 0}\|X(t+s)\|)
\end{aligned} \tag{64}$$

Hence, based on (62) and (64), the two functions, $\underline{\kappa}(\cdot)$ and $\overline{\kappa}(\cdot) \in \mathcal{K}_\infty$, satisfy

$$\underline{\kappa}(\|X(t)\|) \leq V_k(X(t)) \leq \overline{\kappa}(\sup_{-\tau\leq s\leq 0}\|X(t+s)\|) \tag{65}$$

According to the definition (53), it induces

$$V_k(X(t)) \leq \upsilon V_p(X(t)), \ \forall k, p \in \mathbb{M} \tag{66}$$

Let the initial time be t_{s_1}. In the persistence period T-portion from Figure 1, for any $t \in \left[t_{s_{p+1}-1}, t_{s_{p+1}}\right)$, it yields from (60) and (66) that

$$\begin{aligned}
V_{\sigma(t)}(X(t)) &\leq e^{-\beta(t-t_{s_{p+1}-1})}V_{\sigma(t_{s_{p+1}-1})}(X(t_{s_{p+1}-1})) \\
&\quad + \int_{t_{s_{p+1}-1}}^{t}\Theta e^{-\mu(t-\omega)}d\omega \\
&\leq \upsilon e^{-\mu(t-t_{s_{p+1}-1})}V_{\sigma(t^-_{s_{p+1}-1})}(X(t^-_{s_{p+1}-1})) \\
&\quad + \int_{t_{s_{p+1}-1}}^{t}\Theta e^{-\mu(t-\omega)}d\omega \leq \cdots \\
&\leq \upsilon^{N(t_{s_1},t)}e^{-\mu(t-t_{s_1})}V_{\sigma(t_{s_1})}(X(t_{s_1})) \\
&\quad + \int_{t_{s_{p+1}-1}}^{t}\Theta e^{-\mu(t-\omega)}d\omega + \cdots \\
&\quad + \upsilon^{N(t_{s_1},t)}\int_{t_{s_1}}^{t_{s_1+1}}\Theta e^{-\mu(t-\omega)}d\omega
\end{aligned} \tag{67}$$

Inspired by [21], for any $\omega \in \left(t_{s_p+i}, t_{s_d+i+1}\right)$, one gets

$$N(t_{s_p+i}, t) = N(\omega, t) \tag{68}$$

which implies that

$$\begin{aligned}
V_{\sigma(t)}(X(t)) &\leq \upsilon^{N(t_{s_1},t)}e^{-\mu(t-t_{s_1})}V_{\sigma(t_{s_1})}(X(t_{s_1})) \\
&\quad + \int_{t_{s_1}}^{t}\Theta\upsilon^{N(\omega,t)}e^{-\mu(t-\omega)}d\omega
\end{aligned} \tag{69}$$

Based on (3), the first term in (69) can be further obtained as follows:

$$\begin{aligned}
& \upsilon^{N(t_{s_1},t)}e^{-\mu(t-t_{s_1})}V_{\sigma(t_{s_1})}(X(t_{s_1})) \\
& \quad \leq \upsilon^{T\hat{f}+1}e^{\left(\frac{T\hat{f}+1}{\tau_d+T}\ln\upsilon-\mu\right)(t-t_{s_1})}V_{\sigma(t_{s_1})}(X(t_{s_1}))
\end{aligned} \tag{70}$$

To proceed with, the second term in (69) can be shown that

$$\begin{aligned}
& \int_{t_{s_1}}^{t}\Theta\upsilon^{N(\omega,t)}e^{-\mu(t-\omega)}d\omega \\
& \leq \Theta\upsilon^{T\hat{f}+1}\int_{t_{s_1}}^{t}\upsilon^{\frac{T\hat{f}+1}{\tau_d+T}(t-\omega)}e^{-\mu(t-\omega)}d\omega \\
& \leq \frac{\Theta\upsilon^{T\hat{f}+1}}{\frac{T\hat{f}+1}{\tau_d+T}\ln\upsilon-\mu}e^{\left(\frac{T\hat{f}+1}{\tau_d+T}\ln\upsilon-\mu\right)(t-t_{s_1})} - \frac{\Theta\upsilon^{T\hat{f}+1}}{\frac{T\hat{f}+1}{\tau_d+T}\ln\upsilon-\mu}
\end{aligned} \tag{71}$$

By utilizing $(\tau_d + T)/(T\hat{f}+1) \geq (\ln\upsilon)/\mu$, it yields from (70) and (71) that as $t \to \infty$,

$$\begin{aligned}
V_{\sigma(t)}(X(t)) &\leq \upsilon^{T\hat{f}+1}e^{\left(\frac{T\hat{f}+1}{\tau_d+T}\ln\upsilon-\mu\right)(t-t_{s_1})}V_{\sigma(t_{s_1})}(X(t_{s_1})) \\
&\quad + \frac{\Theta\upsilon^{T\hat{f}+1}}{\frac{T\hat{f}+1}{\tau_d+T}\ln\upsilon-\mu}e^{\left(\frac{T\hat{f}+1}{\tau_d+T}\ln\upsilon-\mu\right)(t-t_{s_1})} - \frac{\Theta\upsilon^{T\hat{f}+1}}{\frac{T\hat{f}+1}{\tau_d+T}\ln\upsilon-\mu}
\end{aligned} \tag{72}$$

10991239, 2025, 6, Downloaded from https://onlinelibrary.wiley.com/doi/10.1002/rnc.7765 by HONG KONG POLYTECHNIC UNIVERSITY HU NG HOM, Wiley Online Library on [20/09/2025]. See the Terms and Conditions (https://onlinelibrary.wiley.com/terms-and-conditions) on Wiley Online Library for rules of use; OA articles are governed by the applicable Creative Commons License

Together with (70) and (71), one gets

$$
\begin{aligned}
V_{\sigma(t)}(X(t)) \leq{}& \upsilon^{T\hat{f}+1} e^{\left(\frac{T\hat{f}+1}{\tau_d+T}\ln \upsilon-\mu\right)(t-t_{s_1})} V_{\sigma(t_{s_1})}(X(t_{s_1})) \\
&+ \frac{\Theta \upsilon^{T\hat{f}+1}}{\frac{T\hat{f}+1}{\tau_d+T}\ln \upsilon-\mu} e^{\left(\frac{T\hat{f}+1}{\tau_d+T}\ln \upsilon-\mu\right)(t-t_{s_1})} - \frac{\Theta \upsilon^{T\hat{f}+1}}{\frac{T\hat{f}+1}{\tau_d+T}\ln \upsilon-\mu}
\end{aligned} \tag{73}
$$

which implies for any $t > 0$,

$$
\begin{aligned}
\underline{\kappa}(\|X(t)\|) \leq{}& \upsilon^{T\hat{f}+1} e^{\left(\frac{T\hat{f}+1}{\tau_d+T}\ln \upsilon-\mu\right)(t-t_{s_1})} \overline{\kappa}\Big(\sup_{-\tau\leq\omega\leq t_{s_1}} \|X(\omega)\|\Big) \\
&+ \frac{\Theta \upsilon^{T\hat{f}+1}}{\frac{T\hat{f}+1}{\tau_d+T}\ln \upsilon-\mu} e^{\left(\frac{T\hat{f}+1}{\tau_d+T}\ln \upsilon-\mu\right)(t-t_{s_1})} - \frac{\Theta \upsilon^{T\hat{f}+1}}{\frac{T\hat{f}+1}{\tau_d+T}\ln \upsilon-\mu}
\end{aligned} \tag{74}
$$

Therefore, for any bounded initial values, one can obtain by (73) that if the persistent dwell time satisfies $(\tau_d + T)/(T\hat{f} + 1) \geq (\ln \upsilon)/\mu$, then ε_{il}, z_{il}, $\tilde{\theta}_{il}$, and η_{ij} are bounded for $i = 1, \dots, n$ and $l = 1, \dots, m$. According to the definition of $\tilde{\theta}_{il}$, one can know that $\hat{\theta}_{il}$ is bounded for $i = 1, \dots, n$ and $l = 1, \dots, m$. Then, through (32), (40), and (49), one gets α_{il} and u_{ik} are bounded for $i = 1, \dots, n$, $l = 1, \dots, m-1$, and $k \in \mathbb{M}$. To proceed with (22c), one has ξ_{il} is bounded for $i = 1, \dots, n$ and $l = 2, \dots, m$. Next, based on (22b), $\hat{x}_{il}$ is bounded for $i = 1, \dots, n$ and $l = 2, \dots, m$. According to (13) and (22a), it yields that x_{il} is also bounded for $i = 1, \dots, n$ and $l = 1, \dots, m$. Hence, for $k \in \mathbb{M}$, all signals in the closed-loop system are bounded under a category of switching signals with the persistent dwell time satisfying $(\tau_d + T)/(T\hat{f} + 1) \geq (\ln \upsilon)/\mu$.

2. Let the Lyapunov function be $V_z = \sum_{i=1}^{n}\sum_{j=1}^{m} z_{ij}^2/2$. In what follows, based on (60), one has

$$
\dot{V}_z \leq -\varsigma V_z^{w\prime} + \Upsilon \tag{75}
$$

where $\varsigma = \min\{\overline{c}_{ij},\ i = 1, \dots, n,\ l = 1, \dots, m\}$, $w' = (w+1)/2$, and $\Upsilon = \sum_{i=1}^{n}[m\varrho_i r_{i0} e^{\beta\tau}\|\varepsilon_i\|^2 + e^{-\beta\tau}\sum_{j=1}^{n} F_{i1j}^2(x_j)/(2r_{i1}) + e^{-\beta\tau}\sum_{j=1}^{n} H_{i1j}^2(x_{j\tau})/(2r_{i1}) + \sum_{j=1}^{m}(a_{ij}^2/2 + \delta_{ij}^{*2}/2) + \sum_{j=2}^{m}\eta_{i,j}^2/2]$. Besides, based on (75), a constant c_0 exists and satisfies $c_0 \in (0, 1]$ such that

$$
\dot{V}_z \leq -c_0\varsigma V_z^{w\prime} - (1-c_0)\varsigma V_z^{w\prime} + \Upsilon \tag{76}
$$

To proceed with, if $V_z^{w\prime} > \Upsilon/[(1-c_0)\varsigma]$, then one gets

$$
\dot{V}_z \leq -c_0\varsigma V_z^{w\prime} \tag{77}
$$

According to Lemma 1, the trajectory of z_{ij} can approach $V_z^{w\prime} > \Upsilon/[(1-c_0)\varsigma]$ in the finite time for $i = 1, \dots, n$ and $l = 1, \dots, m$, that is,

$$
\lim_{c_0 \to c_0'} z_{ij} \in \left(V_z^{w\prime} \leq \frac{\Upsilon}{(1-c_0)\varsigma} \right) \tag{78}
$$

where $c_0' \in (0, 1)$. Then, the finite time T_z from (78) is determined as

$$
T_z \leq \frac{V_z^{1-w\prime}(0)}{c_0'(1-w\prime)} \tag{79}
$$

where $V_z(0)$ is the initial value of V_z. Furthermore, recalling Lemma 1, it can be concluded that the signal z_{ij} is semi-global practically finite-time stable for $i = 1, \dots, n$ and $l = 1, \dots, m$. Thus, the tracking error $y_i(t) - y_{ir}(t)$ with $i = 1, \dots, n$ can stay within a small domain of origin in the finite time. The proof has been completed. □

Remark 3. A detailed guideline from Steps 1–5 is provided to elucidate the design of parameters for the proposed output-feedback control strategy.

1. Select the proper parameters L_{ilk}, such that the matrices A_{ik} are Hurwitz for $i = 1, \dots, n$, $l = 1, \dots, m$, and $k \in \mathbb{M}$.
2. Specify the symmetric matrices $B_{ik} > 0$, then the symmetric matrices $P_{ik} > 0$ can be calculated by solving (12).
3. Decide the number of neural network nodes and Gaussian functions, then determine neural networks (5).
4. Select suitable controller design parameters a_{ik}, c_{il}, c_{imk}, $\overline{c}_{il}$, w, ℓ_{il}, ρ_i, and q_{il} for $i = 1, \dots, n$, $l = 1, \dots, m$, and $k \in \mathbb{M}$, and then determine the controllers (32), (40), and (49) with the adaptive laws (33), (41), and (50).
5. Determine the designed parameters of persistent dwell time with $\mu > 0$ in (52) and $\upsilon \geq 1$ in (53).

4 | Case Studies

This section provides case studies to show the effectiveness and flexibility of the proposed decentralized neural output feedback quantized control strategy on the switched nonlinear large-scale delayed system.

Example: Consider two continuous stirred tank reactor systems with recycling depicted in Figure 3. Through two different source streams connected to a supervisor, two exothermic and irreversible reactions occur in two reactors. In both reactors, the cooling jackets are filled with cooled water at flow rates F_{j1} and F_{j2}, temperatures T_{j1} and T_{j2}, respectively. Define $V_{j1} = V_{j2} = V_j$, $V_1 = V_2 = V$, $F_{0k} = F_{2k} = F_k$, and $F_{1k} = F_k + F_{Rk}$ for $k = 1, 2$. According to the mass and energy balances [45], the two

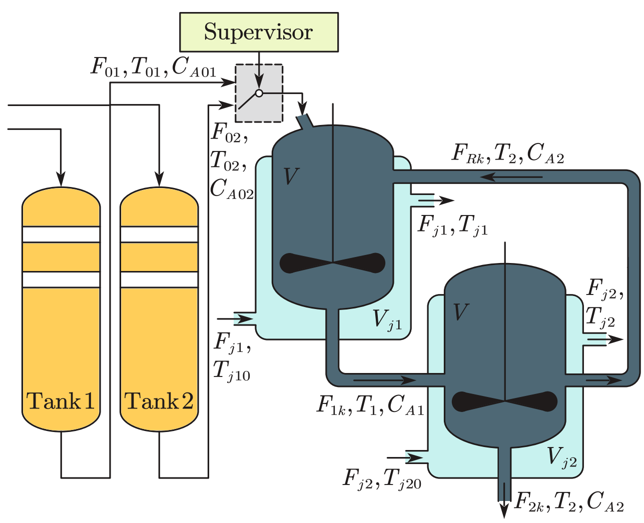

FIGURE 3 | Schematic of two continuous stirred tank reactor systems.

10991239, 2025, 6, Downloaded from https://onlinelibrary.wiley.com/doi/10.1002/rnc.7765 by HONG KONG POLYTECHNIC UNIVERSITY HU NG HOM, Wiley Online Library on [20/09/2025]. See the Terms and Conditions (https://onlinelibrary.wiley.com/terms-and-conditions) on Wiley Online Library for rules of use; OA articles are governed by the applicable Creative Commons License

continuous stirred tank reactor systems with the two switched subsystems are described as follows:

$$\dot{C}_{A1} = \frac{F_{0k}}{V}C_{A0k} - \frac{F_{1k}}{V}C_{A1} + \frac{F_{Rk}}{V}C_{A2} - \overline{\xi}_k C_{A1} e^{-\frac{E_k}{R_k T_1}} \tag{80a}$$

$$\dot{C}_{A2} = \frac{F_{1k}}{V}C_{A1} - \frac{F_{1k}}{V}C_{A2} - \overline{\xi}_k C_{A2} e^{-\frac{E_k}{R_k T_2}} \tag{80b}$$

$$\begin{aligned}\dot{T}_1 = {} & \frac{F_{0k}}{V}T_{0k} - \frac{F_{1k}}{V}T_1 + \frac{F_{Rk}}{V}T_2 - \frac{\overline{\xi}_k \lambda_k}{\rho_{tk} c_{tk}} C_{A1} e^{-\frac{E_k}{R_k T_1}} \\ & - \frac{U_k A_k}{\rho_{tk} c_{tk} V}\left(T_1 - T_{j1}\right)\end{aligned} \tag{80c}$$

$$\dot{T}_2 = \frac{F_{1k}}{V}(T_1 - T_2) - \frac{U_k A_k}{\rho_{tk} c_{tk} V}\left(T_2 - T_{j2}\right) - \frac{\overline{\xi}_k \lambda_k}{\rho_{tk} c_{tk}} C_{A2} e^{-\frac{E_k}{R_k T_2}} \tag{80d}$$

$$\dot{T}_{j1} = \frac{F_{j1}}{V_j}\left(T_{j10} - T_{j1}\right) + \frac{U_k A_k}{\rho_{jk} c_{jk} V_j}\left(T_1 - T_{j1}\right) \tag{80e}$$

$$\dot{T}_{j2} = \frac{F_{j2}}{V_j}\left(T_{j20} - T_{j2}\right) + \frac{U_k A_k}{\rho_{jk} c_{jk} V_j}\left(T_2 - T_{j2}\right) \tag{80f}$$

where $k = 1, 2$. The physical meaning of the corresponding parameters of the system (80) can be found in Reference [45]. Define the system states $x_{11} = C_{A1} - C_{A1}^*$, $x_{12} = C_{A2} - C_{A2}^*$, $x_{21} = T_2 - T_2^*$, $x_{22} = T_{j2} - T_{j2}^*$, $x_{31} = T_1 - T_1^*$, and $x_{32} = T_{j1} - T_{j1}^*$, where $C_{A1}^*, C_{A2}^*, T_1^*, T_2^*, T_{j1}^*$, and T_{j2}^* are the steady-state values. According to locally modal state feedback linearization in References [19, 45], the switched two continuous stirred tank reactor delayed systems with the input hysteresis quantizer can be rewritten as follows:

$$\dot{x}_{11} = x_{12} + \psi_{11k} \tag{81a}$$

$$\dot{x}_{12} = Q(u_{1k}) + \psi_{12k} \tag{81b}$$

$$\dot{x}_{21} = \phi_{21k} x_{22} + \varphi_{21k}(x_{11}, x_{21}, x_{31}) + \psi_{21k} \tag{81c}$$

$$\dot{x}_{22} = Q(u_{2k}) + \varphi_{22k}(x_{21}, x_{22}) + \psi_{22k} \tag{81d}$$

$$\dot{x}_{31} = \phi_{31k} x_{32} + \varphi_{31k}(x_{11}, x_{12}, x_{21}, x_{31}) + \psi_{31k} \tag{81e}$$

$$\dot{x}_{32} = Q(u_{3k}) + \varphi_{32k}(x_{31}, x_{32}) + \psi_{32k} \tag{81f}$$

$$y_1 = x_{11}, y_2 = x_{21}, y_3 = x_{31} \tag{81g}$$

where ψ_{ilk} represents the unmeasured disturbance with time delays of the system (81) for $i = 1, 2, 3$, $l = 1, 2$, and $k = 1, 2$. Suppose that the function ψ_{ilk} satisfy $\psi_{111} = \sin(x_{11\tau} x_{22}) + x_{11}\sin(x_{21\tau} x_{12})$, $\psi_{112} = 0.9\sin(x_{11\tau} x_{22}) + x_{11}\cos(x_{21\tau} x_{12}) - 0.5$, $\psi_{12k} = 0$, $\phi_{211} = 1$, $\phi_{212} = 2$, $\psi_{211} = -\varphi_{211} + x_{31} + x_{21\tau}\sin(e^{x_{12}}) + x_{11}\sin(x_{21\tau} x_{12})$, $\psi_{212} = -\varphi_{212} + x_{31} + 1.2x_{21\tau}\sin(e^{x_{12}}) + x_{11}\cos(x_{21\tau} x_{12})$, $\psi_{221} = -\varphi_{221} + 3.5\sin(x_{21\tau}) + 6\sin(x_{22}) - 2$, $\psi_{222} = -\varphi_{222} + 2\sin(x_{21\tau}) + 7\sin(x_{22}) - 1.5$, $\phi_{311} = 3$, $\phi_{312} = 1$, $\psi_{311} = -\varphi_{311} + x_{32}x_{22}/(3 + x_{31\tau}^2)$, $\psi_{312} = -\varphi_{312} + 1.5\cos(x_{32})x_{22}/(4 + x_{31\tau}^2)$, $\psi_{321} = -\varphi_{321} + x_{31\tau}^3 x_{32}$, and $\psi_{322} = -\varphi_{322} + 0.8x_{31\tau}^3 x_{32}$ with $\tau_1(t) = \tau_2(t) = \tau_3(t) = 0.1(1 + \sin(t)^2)$. Then, for $i = 1, 2, 3$, the switched high-gain quantized state observer is constructed as

$$\dot{\hat{x}}_{i1} = \hat{x}_{i2} + L_{i1k}(y_i - \hat{x}_{i1}) \tag{82a}$$

$$\dot{\hat{x}}_{i2} = Q(u_{ik}) + L_{i2k}(y_i - \hat{x}_{i1}) \tag{82b}$$

To proceed with, the parameters are considered as $L_{i11} = 10$, $L_{i21} = 10$, $L_{i12} = 8$, and $L_{i22} = 8$ such that matrices A_{i1} and A_{i2} are Hurwitz. In addition, one selects $Q_{i1} = 6I_2$ and $Q_{i2} = 5I_2$ with $I_2 = \mathrm{diag}\{1, 1\}$. Meanwhile, the symmetric positive definite matrices are

$$P_{i1} = \begin{bmatrix} 3.3 & -3.00 \\ -3.00 & 3.33 \end{bmatrix}, P_{i2} = \begin{bmatrix} 2.81 & -2.50 \\ -2.50 & 2.85 \end{bmatrix}$$

satisfying (12). Then, the relevant decentralized output-feedback control information is designed as

$$\alpha_{i1} = -\frac{1}{2a_{i1}^2} z_{i1}\hat{\theta}_{i1} S_{i1}^\top S_{i1} - \frac{1}{2}z_{i1} - c_{i1}z_{i1} - \overline{c}_{i1}|z_{i1}|^w \mathrm{sgn}(z_{i1}) \tag{83}$$

$$\dot{\hat{\theta}}_{il} = \frac{\ell_{il}}{2a_{il}^2} z_{il}^2 S_{il}^\top S_{il} - \gamma_{il}\hat{\theta}_{il} \tag{84}$$

$$\begin{aligned} u_{ik} = -\frac{1}{1 - \rho_i}\Bigg[& \frac{1}{2a_{i2}^2} z_{i2}\hat{\theta}_{i2} S_{i2}^\top S_{i2} + \frac{1}{2}z_{i2} \\ & + c_{i2k} z_{i2} + \overline{c}_{i2}|z_{i2}|^w \mathrm{sgn}(z_{i2}) - \dot{\xi}_{i2}\Bigg]\end{aligned} \tag{85}$$

where $i = 1, 2, 3$, $l = 1, 2$, and $k = 1, 2$. The design parameters are chosen as $c_{i1} = 50$, $c_{i21} = 50$, $c_{i22} = 60$, $\overline{c}_{il} = 1.5$, $a_{il} = 10$, $w = 0.5$, $\ell_{il} = 5$, and $\gamma_{il} = 10$ for $i = 1, 2, 3$ and $l = 1, 2$. Also, the parameters of the input hysteresis quantizer are chosen as $\chi_i = 0.4$ and $u_{i,\min} = 25$ for $i = 1, 2, 3$. Then, it can be obtained by (52) and (53) that $\mu = 3.14$ and $\upsilon = 20.05$. Based on Theorem 1, as the relevant parameters of the persistent dwell time are given by $T = 6$ s and $\hat{f} = 1\ \mathrm{s}^{-1}$, the persistent dwell time stratifies $\tau_d = 0.69$.

To proceed with, the basis function vectors $S_{i1}(X_{i1})$ and $S_{i2}(X_{i2})$ contain 15 and 25 nodes, and their centers ϑ_{i1} and ϑ_{i2} evenly spaced in $[-2, 2] \times [-3, 3] \times [-4, 4]$ and $[-6, 2] \times [-3, 3] \times [-8, 3] \times [-3, 6] \times [-5, 7] \times [-2, 3] \times [-4, 8]$ and widths $\iota_{i1} = 5$ and $\iota_2 = 2$ for $i = 1, 2, 3$, respectively. The initial vectors are provided as $x(t_0)^\top = [0.5, 0.2, 0.5, 0.2, 0.5, 0.2]^\top$, $\hat{x}(t_0)^\top = [0.1, 0.2, 0.1, 0.2, 0.1, 0.2]^\top$, $\hat{\theta}_{i1}(t_0) = 0.5$, and $\hat{\theta}_{i2}(t_0) = 0.3$ for $i = 1, 2, 3$ with $t_0 \in [-0.2, 0]$. The reference signals are $y_{1r} = 0.5\cos(0.5t)$, $y_{2r} = 0.2\sin(3t) + 0.5\cos(0.5t)$, and $y_{3r} = 0.5\cos(0.8t)$. The test results of system (81) are shown in Figures 4–13. It is clear that, as observed from the figures, all signals in the closed-loop switched system are bounded. The chattering phenomenon observed in the control inputs, as shown in Figures 11–13, can be attributed to the following factors: (1) While the dynamic surface control technique simplifies the derivative computation in the backstepping method, the low-pass filters introduced in this design may induce high-frequency chattering due to their inherent dynamic characteristics; (2) Quantization errors reduce the estimation accuracy of the state observer to balance control input signal and computing resource constraints, which may contribute to chattering. The chattering phenomenon is a cumulative result

10991239, 2025, 6, Downloaded from https://onlinelibrary.wiley.com/doi/10.1002/rnc.7765 by HONG KONG POLYTECHNIC UNIVERSITY HU NG HOM, Wiley Online Library on [20/09/2025]. See the Terms and Conditions (https://onlinelibrary.wiley.com/terms-and-conditions) on Wiley Online Library for rules of use; OA articles are governed by the applicable Creative Commons License

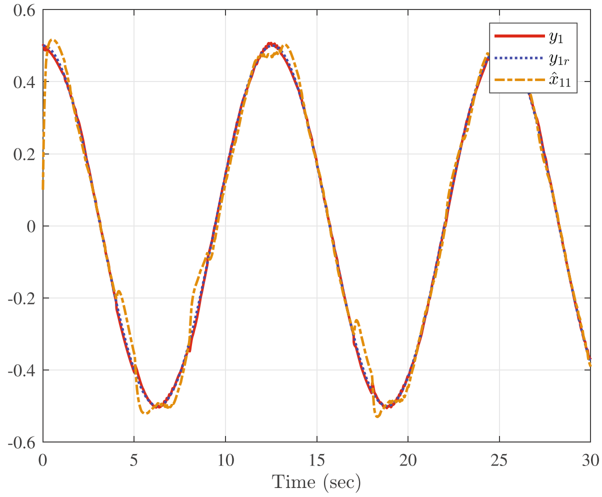

FIGURE 4 | The system output y_1, the reference signal y_{1r}, and the observer state $\hat{x}_{11}$.

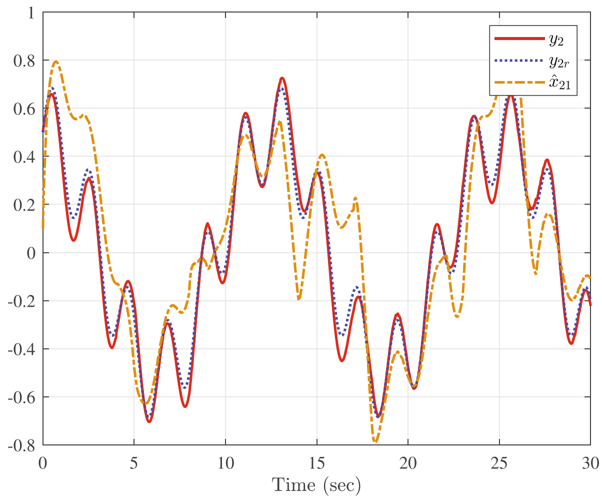

FIGURE 5 | The system output y_2, the reference signal y_{2r}, and the observer state $\hat{x}_{21}$.

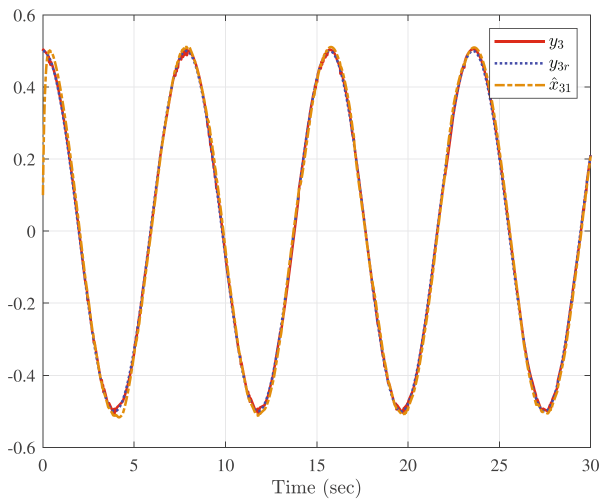

FIGURE 6 | The system output y_3, the reference signal y_{3r}, and the observer state $\hat{x}_{31}$.

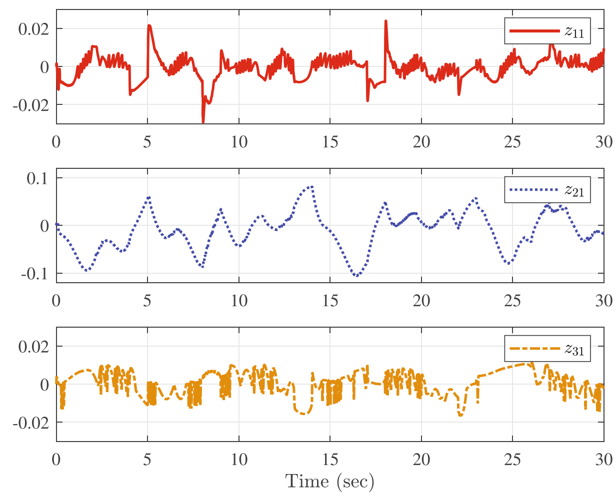

FIGURE 7 | The tracking errors z_{11}, z_{21}, and z_{31}.

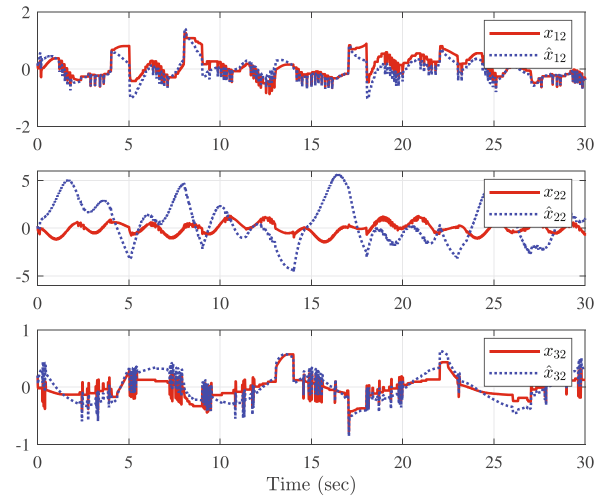

FIGURE 8 | The system states x_{12}, x_{22}, x_{32}, and the observer states $\hat{x}_{12}$, $\hat{x}_{22}$, $\hat{x}_{32}$.

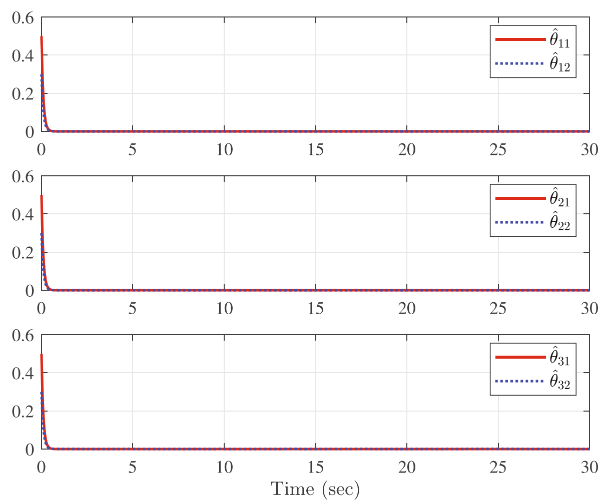

FIGURE 9 | The adaptive laws $\hat{\theta}_{il}$ with $i = 1, 2, 3$ and $l = 1, 2$.

10991239, 2025, 6, Downloaded from https://onlinelibrary.wiley.com/doi/10.1002/rnc.7765 by HONG KONG POLYTECHNIC UNIVERSITY HU NG HOM, Wiley Online Library on [20/09/2025]. See the Terms and Conditions (https://onlinelibrary.wiley.com/terms-and-conditions) on Wiley Online Library for rules of use; OA articles are governed by the applicable Creative Commons License

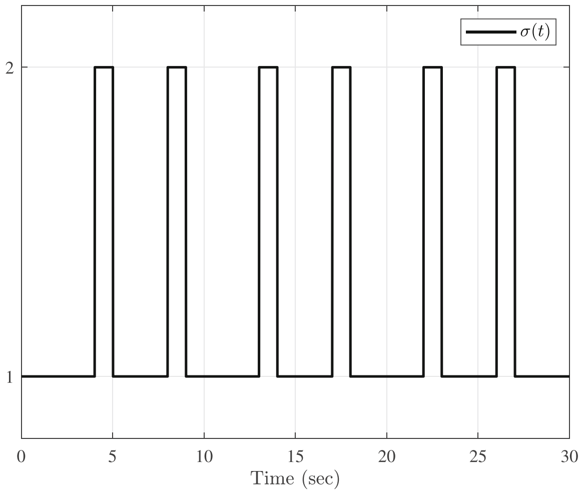

FIGURE 10 | The switching signal $\sigma(t)$ under the persistent dwell time.

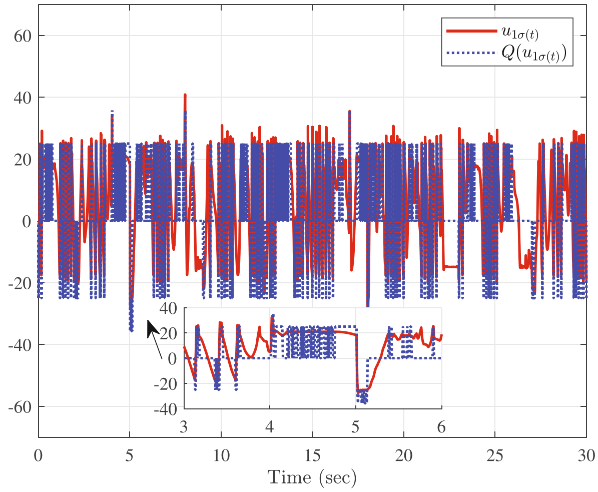

FIGURE 11 | The control input $u_{1\sigma(t)}$ and the quantized control input $Q(u_{1\sigma(t)})$.

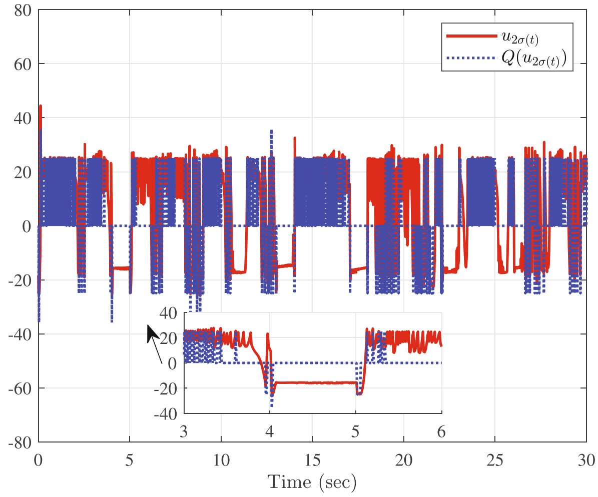

FIGURE 12 | The control input $u_{2\sigma(t)}$ and the quantized control input $Q(u_{2\sigma(t)})$.

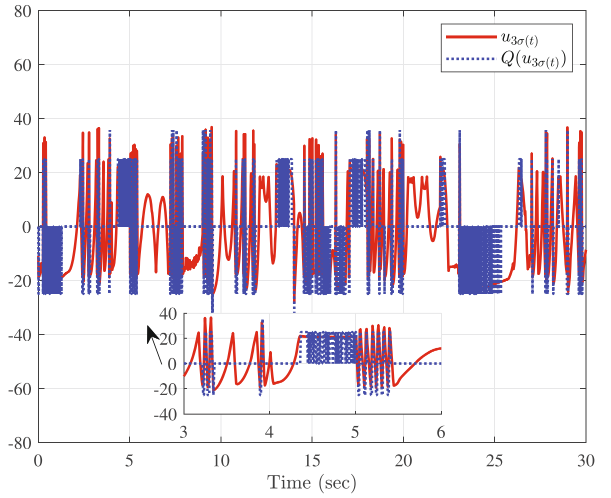

FIGURE 13 | The control input $u_{3\sigma(t)}$ and the quantized control input $Q(u_{3\sigma(t)})$.

of these various effects, reflecting the trade-offs between control objectives and computing resources. Besides, the output tracking error $y_i - y_{ir}$ for $i = 1, 2, 3$ converges to a small domain of origin in finite time under a category of switching signals with the persistent dwell time.

5 | Conclusion

In this paper, a decentralized finite-time adaptive neural output-feedback quantized control scheme has been developed for a class of switched nonlinear large-scale delayed systems. By introducing the proper multiple Lyapunov–Krasovskii functions, all the signals in the closed-loop system are semi-globally uniformly ultimate bounded under a category of switching signals with the persistent dwell time via the dynamic surface control technique. It has been demonstrated that the tracking error can stay in a small neighborhood of origin in finite time despite the effects of the time-varying delays.

Acknowledgments

This paper was supported in part by the National Science and Technology Major Project under Grant 2022ZD0119900, in part by the National Natural Science Foundation of China under Grant U2141234, Grant U24A20260, and Grant 62303308, in part by the Hainan Province Science and Technology Special Fund under Grant ZDYF2024GXJS003, in part by Shanghai Pujiang Program under Grant 23PJ1404700, in part by Joint Research Fund of Shanghai Academy of Spaceflight Technology under Grant USCAST2023-22, and in part by the Hainan Special PhD Scientific Research Foundation of Sanya Yazhou Bay Science and Technology City under Grant HSPHDSRF-2022-01-005.

Conflicts of Interest

The authors declare no conflicts of interest.

Data Availability Statement

Data sharing is not applicable to this article as no new data were created or analyzed in this study.

10991239, 2025, 6, Downloaded from https://onlinelibrary.wiley.com/doi/10.1002/rnc.7765 by HONG KONG POLYTECHNIC UNIVERSITY HU NG HOM, Wiley Online Library on [20/09/2025]. See the Terms and Conditions (https://onlinelibrary.wiley.com/terms-and-conditions) on Wiley Online Library for rules of use; OA articles are governed by the applicable Creative Commons License

References

1. X. Yang, Y. Ge, W. Deng, and J. Yao, "Command Filtered Adaptive Tracking Control of Nonlinear Systems With Prescribed Performance Under Time-Variant Parameters and Input Delay," *International Journal of Robust and Nonlinear Control* 33, no. 4 (2022): 2840–2860.

2. Z. Li, G. Cao, W. Xie, R. Gao, and W. Zhang, "Switched-Observer-Based Adaptive Neural Networks Tracking Control for Switched Nonlinear Time-Delay Systems With Actuator Saturation," *Information Sciences* 621 (2023): 36–57.

3. W. Zhou, J. Fu, H. Yan, X. Du, Y. Wang, and H. Zhou, "Event-Triggered Approximate Optimal Path-Following Control for Unmanned Surface Vehicles With State Constraints," *IEEE Transactions on Neural Networks and Learning Systems* 34, no. 1 (2023): 104–118.

4. H. Chen, Z. Liu, C. Alippi, B. Huang, and D. Liu, "Explainable Intelligent Fault Diagnosis for Nonlinear Dynamic Systems: From Unsupervised to Supervised Learning," *IEEE Transactions on Neural Networks and Learning Systems* 35, no. 5 (2024): 6166–6179.

5. K. Xu, H. Wang, and P. X. Liu, "Singularity-Free Adaptive Fixed-Time Tracking Control for MIMO Nonlinear Systems With Dynamic Uncertainties," *IEEE Transactions on Circuits and Systems II: Express Briefs* 71, no. 3 (2024): 1356–1360.

6. T. Zhang and T. Liu, "Adaptive Neural Optimal Control via Command Filter for Nonlinear Multi-Agent Systems Including Time-Varying Output Constraints," *International Journal of Robust and Nonlinear Control* 33, no. 2 (2023): 820–849.

7. D. Swaroop, J. K. Hedrick, P. P. Yip, and J. C. Gerdes, "Dynamic Surface Control for a Class of Nonlinear Systems," *IEEE Transactions on Automatic Control* 45, no. 10 (2000): 1893–1899.

8. Q. Zeng, Y. J. Liu, and L. Liu, "Adaptive Vehicle Stability Control of Half-Car Active Suspension Systems With Partial Performance Constraints," *IEEE Transactions on Systems, Man, and Cybernetics: Systems* 51, no. 3 (2021): 1704–1714.

9. S. Yuan, L. Zhang, B. De Schutter, and S. Baldi, "A Novel Lyapunov Function for a Non-weighted L_2 Gain of Asynchronously Switched Linear Systems," *Automatica* 87 (2018): 310–317.

10. Z. Li, H. Chen, W. Wu, and W. Zhang, "Dynamic Output Feedback Fault-Tolerant Control for Switched Vehicle Active Suspension Delayed Systems," *IEEE Transactions on Vehicular Technology* 73, no. 8 (2024): 11059–11071.

11. F. Wang and L. Long, "Dwell-Time-Based Event-Triggered Adaptive Control for Switched Strict-Feedback Nonlinear Systems," *International Journal of Robust and Nonlinear Control* 30, no. 17 (2020): 7052–7073.

12. B. Jiang, Q. Shen, and P. Shi, "Neural-Networked Adaptive Tracking Control for Switched Nonlinear Pure-Feedback Systems Under Arbitrary Switching," *Automatica* 61 (2015): 119–125.

13. J. Zhao and D. J. Hill, "On Stability, L_2-Gain and H_∞ Control for Switched Systems," *Automatica* 44 (2008): 1220–1232.

14. S. Yuan, M. Lv, S. Baldi, and L. Zhang, "Lyapunov-Equation-Based Stability Analysis for Switched Linear Systems and Its Application to Switched Adaptive Control," *IEEE Transactions on Automatic Control* 66, no. 5 (2021): 2250–2256.

15. Z. Li, L. Long, and J. Zhao, "Linear Output-Feedback-Based Semi-Global Stabilization for Switched Nonlinear Time-Delay Systems," *Journal of the Franklin Institute* 356, no. 13 (2019): 7224–7245.

16. D. Liberzon, *Switching in Systems and Control* (Boston, MA, USA: Birkhäuser, 2003).

17. S. Yuan, L. Zhang, and S. Baldi, "Adaptive Stabilization of Impulsive Switched Linear Time-Delay Systems: A Piecewise Dynamic Gain Approach," *Automatica* 103 (2019): 322–329.

18. Z. Li, D. Yue, Y. Ma, and J. Zhao, "Neural-Networks-Based Prescribed Tracking for Nonaffine Switched Nonlinear Time-Delay Systems," *IEEE Transactions on Cybernetics* 52, no. 7 (2022): 6579–6590.

19. L. J. Long and J. Zhao, "Robust Stabilisation of Non-triangular Multi-Input Switched Non-linear Systems and Its Application to a Continuously Stirred Tank Reactor System," *IET Control Theory & Applications* 7, no. 5 (2013): 697–706.

20. J. P. Hespanha, "Uniform Stability of Switched Linear Systems: Extensions of LaSalle's Invariance Principle," *IEEE Transactions on Automatic Control* 49, no. 4 (2004): 470–482.

21. L. Zhang, S. Zhuang, and P. Shi, "Non-weighted Quasi-Time-Dependent H_∞ Filtering for Switched Linear Systems With Persistent Dwell-Time," *Automatica* 54 (2015): 201–209.

22. F. Wang and L. Long, "Event-Triggered Adaptive NN Control for MIMO Switched Nonlinear Systems With Non-ISpS Unmodeled Dynamics," *Journal of the Franklin Institute* 359, no. 4 (2022): 1457–1485.

23. G. X. Zhong and G. H. Yang, "Dynamic Output Feedback Control of Saturated Switched Delay Systems Under the PDT Switching," *International Journal of Robust and Nonlinear Control* 27, no. 15 (2017): 2567–2588.

24. Z. Li, H. Chen, H. K. Lam, W. Wu, and W. Zhang, "Switched Command-Filtered-Based Adaptive Fuzzy Output-Feedback Funnel Control for Switched Nonlinear MIMO Delayed Systems," *IEEE Transactions on Fuzzy Systems* 32, no. 11 (2024): 6560–6572, https://doi.org/10.1109/TFUZZ.2024.3434711.

25. Y. Liu and Q. Zhu, "Event-Triggered Adaptive Neural Network Control for Stochastic Nonlinear Systems With State Constraints and Time-Varying Delays," *IEEE Transactions on Neural Networks and Learning Systems* 34, no. 4 (2023): 1932–1944.

26. J. Mao, W. Zou, W. He, and Z. Xiang, "Practical Finite-Time Sampled-Data Output Feedback Stabilization for a Class of Upper-Triangular Nonlinear Systems With Input Delay," *IEEE Transactions on Systems, Man, and Cybernetics: Systems* 53, no. 6 (2023): 3428–3439.

27. Y. Li, S. Tong, and T. Li, "Adaptive Fuzzy Output Feedback Dynamic Surface Control of Interconnected Nonlinear Pure-Feedback Systems," *IEEE Transactions on Cybernetics* 45, no. 1 (2015): 138–149.

28. Z. Li and L. Long, "Global Stabilization of Switched Feedforward Nonlinear Time-Delay Systems Under Asynchronous Switching," *IEEE Transactions on Circuits and Systems I: Regular Papers* 67, no. 2 (2020): 711–724.

29. Z. Shi, C. Zhou, and J. Guo, "Observer-Based Consensus Tracking Control for a Class of Nonstrict-Feedback Nonlinear Multi-Agent Systems With Prescribed Performance and Input Quantization," *International Journal of Robust and Nonlinear Control* 32, no. 18 (2022): 10374–10395.

30. X. Xia, T. Zhang, Y. Fang, and G. Kang, "Adaptive Quantized Control of Output Feedback Nonlinear Systems With Input Unmodeled Dynamics Based on Backstepping and Small-Gain Method," *IEEE Transactions on Systems, Man, and Cybernetics: Systems* 51, no. 9 (2021): 5686–5697.

31. B. Niu, H. Li, T. Qin, and H. R. Karimi, "Adaptive NN Dynamic Surface Controller Design for Nonlinear Pure-Feedback Switched Systems With Time-Delays and Quantized Input," *IEEE Transactions on Systems, Man, and Cybernetics: Systems* 48, no. 10 (2018): 1676–1688.

32. H. Wang, M. Chen, and P. X. Liu, "Fuzzy Adaptive Fixed-Time Quantized Feedback Control for a Class of Nonlinear Systems," *Zidonghua Xuebao/Acta Automatica Sinica* 47, no. 12 (2021): 2823–2830.

33. J. Li, R. Ji, X. Liang, S. S. Ge, and H. Yan, "Command Filter-Based Adaptive Fuzzy Finite-Time Output Feedback Control of Nonlinear Electrohydraulic Servo System," *IEEE Transactions on Instrumentation and Measurement* 71 (2022): 1–10.

10991239, 2025, 6, Downloaded from https://onlinelibrary.wiley.com/doi/10.1002/rnc.7765 by HONG KONG POLYTECHNIC UNIVERSITY HU NG HOM, Wiley Online Library on [20/09/2025]. See the Terms and Conditions (https://onlinelibrary.wiley.com/terms-and-conditions) on Wiley Online Library for rules of use; OA articles are governed by the applicable Creative Commons License

34. H. Sun, L. Hou, and Y. Wei, "Decentralized Dynamic Event-Triggered Output Feedback Adaptive Fixed-Time Funnel Control for Interconnection Nonlinear Systems," *IEEE Transactions on Neural Networks and Learning Systems* 35, no. 1 (2024): 1364–1378.

35. H. Wang, K. Xu, and H. Zhang, "Adaptive Finite-Time Tracking Control of Nonlinear Systems With Dynamics Uncertainties," *IEEE Transactions on Automatic Control* 68, no. 9 (2023): 5737–5744.

36. W. Wu, Y. Zhang, W. Zhang, and W. Xie, "Output-Feedback Finite-Time Safety-Critical Coordinated Control of Path-Guided Marine Surface Vehicles Based on Neurodynamic Optimization," *IEEE Transactions on Systems, Man, and Cybernetics: Systems* 53, no. 3 (2023): 1788–1800.

37. N. Zhang, J. Xia, J. H. Park, J. Zhang, and H. Shen, "Improved Disturbance Observer-Based Fixed-Time Adaptive Neural Network Consensus Tracking for Nonlinear Multi-Agent Systems," *Neural Networks* 162 (2023): 490–501.

38. C. Fu, Q. G. Wang, J. Yu, and C. Lin, "Neural Network-Based Finite-Time Command Filtering Control for Switched Nonlinear Systems With Backlash-Like Hysteresis," *IEEE Transactions on Neural Networks and Learning Systems* 32, no. 7 (2021): 3268–3273.

39. S. Kamali, S. M. Tabatabaei, M. M. Arefi, and S. Yin, "Prescribed Performance Quantized Tracking Control for a Class of Delayed Switched Nonlinear Systems With Actuator Hysteresis Using a Filter-Connected Switched Hysteretic Quantizer," *IEEE Transactions on Neural Networks and Learning Systems* 33, no. 1 (2022): 61–74.

40. Z. Yu, Y. Yang, S. Li, and J. Sun, "Observer-Based Adaptive Finite-Time Quantized Tracking Control of Nonstrict-Feedback Nonlinear Systems With Asymmetric Actuator Saturation," *IEEE Transactions on Systems, Man, and Cybernetics: Systems* 50, no. 11 (2020): 4545–4556.

41. J. Zhang, S. Li, C. K. Ahn, and Z. Xiang, "Decentralized Event-Triggered Adaptive Fuzzy Control for Nonlinear Switched Large-Scale Systems With Input Delay via Command-Filtered Backstepping," *IEEE Transactions on Fuzzy Systems* 30, no. 6 (2022): 2118–2123.

42. L. J. Long and J. Zhao, "Decentralized Adaptive Neural Output-Feedback DSC for Switched Large-Scale Nonlinear Systems," *IEEE Transactions on Cybernetics* 47, no. 4 (2017): 908–919.

43. H. Du, S. Li, and C. Qian, "Finite-Time Attitude Tracking Control of Spacecraft With Application to Attitude Synchronization," *IEEE Transactions on Automatic Control* 56, no. 11 (2011): 2711–2717.

44. L. Xing, C. Wen, H. Su, Z. Liu, and J. Cai, "Robust Control for a Class of Uncertain Nonlinear Systems With Input Quantization," *International Journal of Robust and Nonlinear Control* 26, no. 8 (2016): 1585–1596.

45. X. Liu, A. Jutan, and S. Rohani, "Almost Disturbance Decoupling of MIMO Nonlinear Systems and Application to Chemical Processes," *Automatica* 40, no. 3 (2004): 465–471.

10991239, 2025, 6, Downloaded from https://onlinelibrary.wiley.com/doi/10.1002/rnc.7765 by HONG KONG POLYTECHNIC UNIVERSITY HU NG HOM, Wiley Online Library on [20/09/2025]. See the Terms and Conditions (https://onlinelibrary.wiley.com/terms-and-conditions) on Wiley Online Library for rules of use; OA articles are governed by the applicable Creative Commons License